The transmission of nuclear pore complexes to daughter cells requires a cytoplasmic pool of Nsp1

Paolo Colombi, Brant M. Webster, Florian Fröhlich, and C. Patrick Lusk

Department of Cell Biology, Yale School of Medicine, New Haven, CT 06520

Nuclear pore complexes (NPCs) are essential protein assemblies that span the nuclear envelope and establish nuclear–cytoplasmic compartmentalization. We have investigated mechanisms that control NPC number in mother and daughter cells during the asymmetric division of budding yeast. By simultaneously tracking existing NPCs and newly synthesized NPC protomers (nups) through anaphase, we uncovered a pool of the central channel nup Nsp1 that is actively targeted to the bud in association with endoplasmic reticulum. Bud targeting required an intact actin cytoskeleton and the class V myosin, Myo2. Selective inhibition of cytoplasmic Nsp1 or inactivation of Myo2 reduced the inheritance of NPCs in daughter cells, leading to a daughter-specific loss of viability. Our data are consistent with a model in which Nsp1 releases a barrier that otherwise prevents NPC passage through the bud neck. It further supports the finding that NPC inheritance, not de novo NPC assembly, is primarily responsible for controlling NPC number in daughter cells.

Introduction

Asymmetric cell divisions are critical for cell fate determination during embryogenesis, organogenesis, and differentiation (Neumüller and Knoblich, 2009). Since the budding yeast *Saccharomyces cerevisiae* undergoes an asymmetric division, it is an effective model for identifying factors that are actively segregated along the polarity axis and the underlying molecular mechanisms responsible for their segregation (Pruyne et al., 2004). In yeast, the two type V myosin motors Myo2 and Myo4 deliver organelles, secretory vesicles, and mRNAs to the daughter cell (Pruyne et al., 2004; Chung and Takizawa, 2010; Eves et al., 2012). Myo2 also plays a role in nuclear migration by guiding spindle microtubules along actin cables in concert with a complex of proteins at the plus ends of microtubules, including Kar9 and Bim1 (Korinek et al., 2000; Miller et al., 2000; Yin et al., 2000). A redundant nuclear positioning pathway requires the dynein–dynactin complex (Eshel et al., 1993; Li et al., 1993; Grava et al., 2006). Recent data also implicates the exocyst complex in anchoring ER tubules that extend from the mother nuclear envelope (NE) to the bud cortex in maintaining nuclear position at the bud neck (Kirchenbauer and Liakopoulos, 2013). Further, the ubiquitylation of a component of the nuclear pore complex (NPC) was shown to function in nuclear migration through the recruitment of dynein light chain to the NE (Hayakawa et al., 2012). The latter process reflects several connections uncovered between NPCs and the cytoskeleton (Stelter et al., 2007; Splinter et al., 2010; Bolhy et al., 2011; Steinberg et al., 2012).

NPCs are massive protein assemblies embedded in the NE that control the flux of molecules between the nucleus and cytoplasm. Each NPC is composed of ∼30 individual protomers termed nucleoporins (nups; Rout et al., 2000; Cronshaw et al., 2002) found in distinct subcomplexes (Siniossoglou et al., 1996, 2000; Grandi et al., 1997; Marelli et al., 1998; Belgareh et al., 2001; Vasu et al., 2001; Alber et al., 2007a,b; Onischenko et al., 2009). These subcomplexes are thought to form modular building blocks that contribute to the formation of the concentric membrane, inner and outer ring complexes that surround a central transport channel (Alber et al., 2007a,b). The channel itself is rich in unstructured nups like Nsp1/Nup62 that contain repetitive peptide motifs of Phe-Gly (FG-nups; Alber et al., 2007a,b). Nsp1 helps form two subcomplexes at the NPC composed of Nup49, Nup57, and Nic96, or Nup82 and Nup159 (Nehrbass et al., 1990; Mutvei et al., 1992; Grandi et al., 1995; Schlaich et al., 1997; Bailer et al., 2000, 2001).

Correspondence to C. Patrick Lusk: patrick.lusk@yale.edu

Abbreviations used in this paper: EBD, Estradiol-binding domain; *mfi*, mean fluorescence intensity; NE, nuclear envelope; NP, nucleopodia; NPC, nuclear pore complex; nup, nucleoporin; RITE, recombination induced tag exchange; *tf*, total nuclear fluorescence.
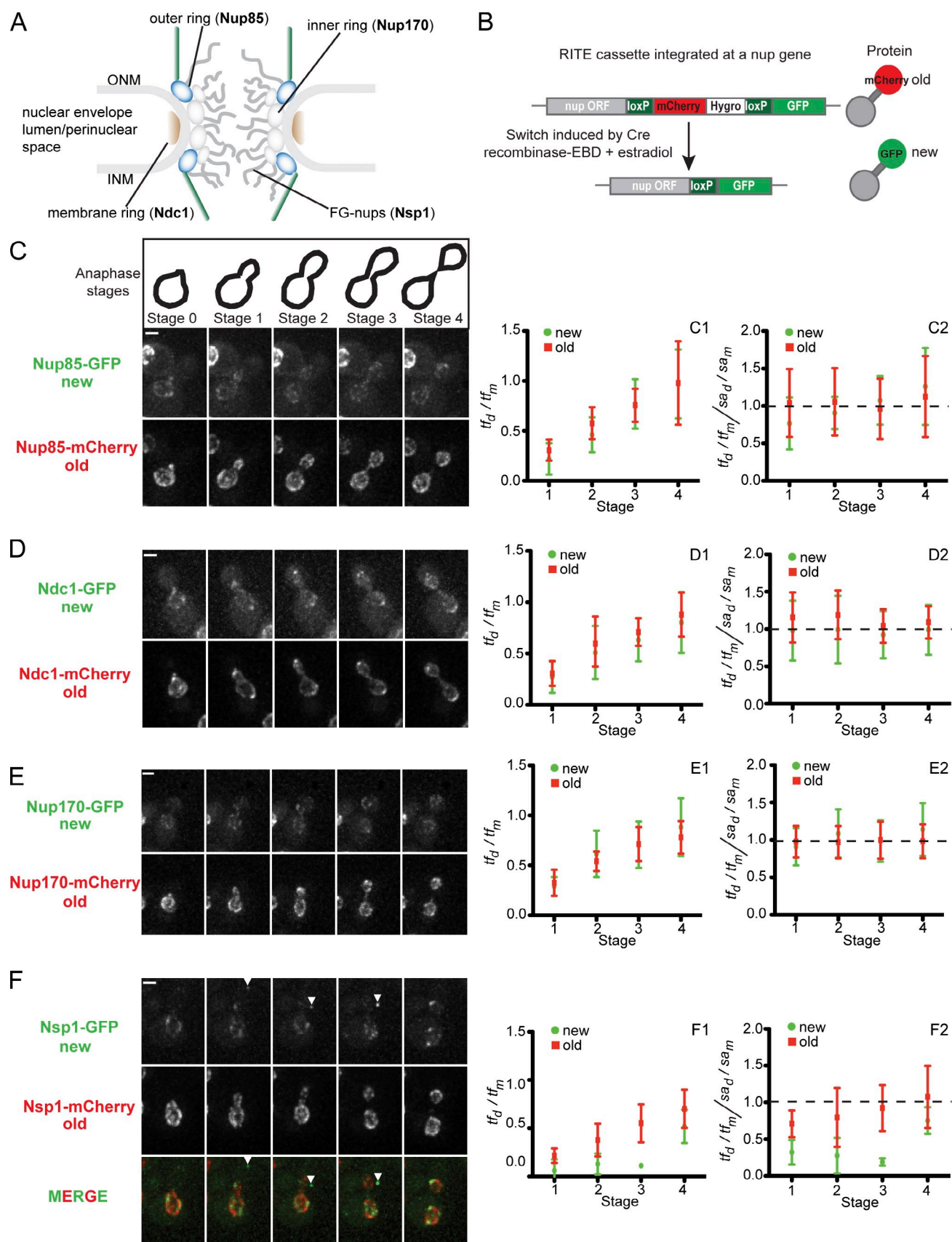
Figure 1. **A newly synthesized bud-directed pool of Nsp1.** (A) Schematic of the NPC with major structural units and representative nups indicated in bold. ONM and INM, outer and inner nuclear membrane, respectively. (B) Schematic of the RITE cassette inserted in frame at the 3′ end of nup genes. Nup-mCherry fusions (old) are produced in cells. The addition of estradiol releases a Cre recombinase–EBD fusion that promotes loxP-mediated recombination,

Because transport through NPCs is essential for cell life, there are likely mechanisms to ensure that NPC numbers can accommodate cell type–specific nuclear transport loads. We understand little about mechanisms that control NPC number. Lymphocyte stimulation results in a doubling of NPC number, which suggests that external inputs can up-regulate the NPC assembly pathway (Maul et al., 1972). Further, the S-phase doubling of NPCs observed in cell culture suggests that NPC assembly is linked to the cell cycle (Maul et al., 1972), perhaps through cyclin-dependent kinases (Maeshima et al., 2010). Mutations in nups important for NPC assembly can also impact differentiation programs (Lupu et al., 2008; de Jong-Curtain et al., 2009; D'Angelo et al., 2012). These studies cumulatively suggest that NPCs themselves might be important for cell fate determination and underscore the importance of identifying mechanisms that control NPC number.

One way to modulate NPC number is to regulate the de novo assembly of NPCs, which occurs by postmitotic and interphase mechanisms (Doucet et al., 2010). During de novo NPC assembly in interphase, the membrane and inner ring complexes assemble at the NE first and might directly contribute to fusion of the inner and outer nuclear membranes (Makio et al., 2009; Onischenko et al., 2009; Doucet et al., 2010; Dultz and Ellenberg, 2010; Fichtman et al., 2010; Vollmer et al., 2012). Other conserved ER and inner nuclear membrane proteins might also act at these early steps (Dawson et al., 2009; Chadrin et al., 2010; Talamas and Hetzer, 2011; Yewdell et al., 2011), which are followed by the recruitment of the outer ring complex, Nic96, and the FG-nups (Zabel et al., 1996; Doucet et al., 2010).

Since budding yeast NEs/NPCs remain intact during mitosis, determining NPC number relies on both de novo assembly and mechanisms that segregate NPCs between mother and daughter cells. One study suggests that mother NPCs are restricted from being inherited by the daughter, placing a burden on de novo NPC assembly to support daughter viability (Shcheprova et al., 2008). Since the known NPC assembly mechanism is relatively slow compared to yeast mitosis (Winey et al., 1997; Dultz and Ellenberg, 2010), there might be a faster daughter-specific NPC assembly mechanism that has yet to be uncovered. It is also plausible that there is a mechanism that ensures NPC inheritance. Such mechanisms exist for several organelles including mitochondria (Itoh et al., 2002), vacuoles (Hill et al., 1996), peroxisomes (Hoepfner et al., 2001; Fagarasanu et al., 2006), cortical ER (Du et al., 2001; Estrada et al., 2003) and late Golgi (Rossanese et al., 2001). Consistent with the idea that NPCs are also actively transmitted to daughter cells, the use of a tandem fluorescent "timer" protein showed a bias of "old" nups in daughters (Khmelinskii et al., 2012).

In an effort to identify putative inheritance and/or de novo NPC assembly mechanisms needed to ensure that adequate numbers of NPCs are present in daughter cells, we investigated the distribution of newly synthesized and assembled pools of representative components of distinct nup subcomplexes through mitotic divisions in budding yeast. We identified a newly synthesized pool of the nup Nsp1 that accumulates between S and G2 phase and is directed into the bud by interactions with ER in a pathway that requires Myo2. Inactivation of newly synthesized Nsp1 results in a dramatic loss of NPC inheritance by daughter cells. Our data are consistent with a model in which Nsp1 is a critical player in a pathway governing NPC number in daughter cells, which ensures their viability.
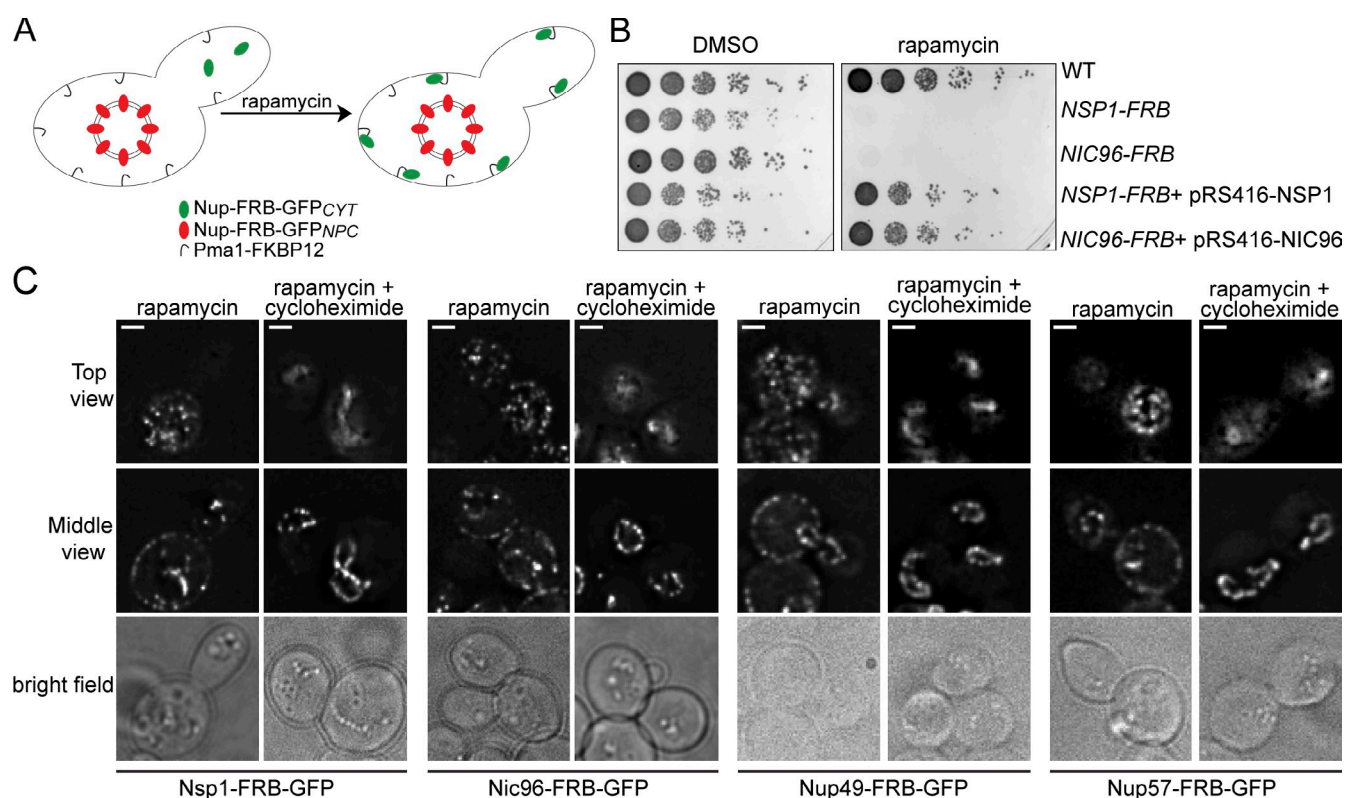
Results

Bud-directed distribution of newly synthesized Nsp1

To investigate how budding yeast nups are segregated between mother and daughter cells, we visualized both newly synthesized and existing pools of representative members of the membrane (Ndc1) and inner (Nup170) and outer ring (Nup85) complexes, in addition to the FG-nup Nsp1 (Fig. 1 A) using a recombination induced tag exchange (RITE) approach (Fig. 1 B; Verzijlbergen et al., 2010). Nup-RITE fusions are expressed from their endogenous gene loci, and tag exchange between mCherry and GFP genes is initiated by an estradiol-induced activation of a constitutively expressed Cre recombinase–estradiol-binding domain (EBD) fusion (Fig. 1 B; Logie and Stewart, 1995). Unlike photoconvertible proteins like Dendra2, which mature slowly ($t_{1/2}$ of maturation ∼1.5 h; Zhang et al., 2007), the RITE approach leverages the fast maturation of GFP ($t_{1/2}$ of maturation <15 min; Iizuka et al., 2011) to visualize the production of "new" nups. Further, the "old" mCherry signal did not increase after the first appearance of "new" green fluorescence, which supports the finding that we can accurately assess the distribution of both old and new versions of these nups through anaphase (Fig. S1).

Consistent with published data (Khmelinskii et al., 2010), we observed that the "old" mCherry nups segregated with the NE (Fig. 1, C–F, bottom panels), which suggests that NPCs are inherited by daughter cells. We simultaneously visualized the appearance and segregation of the "new" GFP nups. Since the genetic switch is not synchronous between cells, we focused on those in which green fluorescence appeared late in the cell cycle to enable the visualization of NPC protomers rather than newly assembled NPCs. GFP fusions of Nup85, Ndc1, and Nup170 segregated equivalently to their "old" counterparts, as reflected in similar daughter/mother total nuclear fluorescence ratios (tf_d/tf_m)

which leads to the replacement of the mCherry gene with a GFP ORF and the production of a nup-GFP (new) protein. (C–F) Cells expressing the indicated Nup-RITE fusions (PCCPL520, PCCPL522, PCCPL526, and WZCPL2) were incubated in the presence of estradiol, and both Nup-GFP and Nup-mCherry were imaged every 3 min through the indicated anaphase stages. Each fluorescence micrograph is a maximum-intensity projection of a deconvolved z series. Note the arrowhead in F showing a bud-localized focus of Nsp1 that does not colocalize with the NE until the last time point (see MERGE and Video 1). C1–F2 are plots (left) of a ratio of *tf* (green and red) in daughters (tf_d) versus mothers (tf_m). These ratios were then divided by a ratio of the surface area of the proportion of the dividing nucleus (through a middle z plane) found in either the daughter (sa_d) or mother (sa_m) to yield plots at right. $6 \leq n \leq 13$. Error bars represent the standard deviation from the mean value. Bars, 2 µm.

Figure 2. **Conditional and specific trapping of newly synthesized nups.** (A) Schematic of the "anchor-away" strategy where nup genes are genomically tagged with ORFs encoding FRB or FRB-GFP and expressed in cells containing a plasma membrane–localized anchor (Pma1-FKBP12; hook). In the presence of rapamycin, only newly synthesized/cytoplasmic nups (Nup-FRB-GFP$_{CYT}$, green ovals) are sequestered, but not those bound to NPCs (Nup-FRB-GFP$_{NPC}$, red ovals). (B) Yeast strains containing the indicated Nup-FRB fusions (PCCPL260, PCCPL251) with wild-type control (HHY110), and indicated plasmids were plated in 10-fold serial dilutions on YPD plates containing rapamycin or carrier (DMSO) and imaged after 48 h at 30°C. (C) Deconvolved fluorescence micrographs (with bright field) of a top and middle z section of cells expressing the indicated Nup-FRB-GFP fusions (PCCPL259, PCCPL302, CPL1238, and CPL1239) incubated for 4 h with rapamycin or with rapamycin and cycloheximide. Bars, 2 μm.

of red and green proteins (Fig. 1, C1, D1, and E1). To normalize for the amount of NE in the daughter and mother, we divided the tf_d/tf_m ratio for a given daughter–mother pair by a daughter/mother ratio of nuclear surface area (sa_d/sa_m). In general, this number hovers around unity for both the newly synthesized and old nups, which indicates a strong correspondence between NE surface area and the number of NPCs (Fig. 1, C2, D2, and E2). These data suggest that for the membrane and inner and outer ring complexes (the scaffold of the NPC), there is little bias in the enrichment of these NPC protomers in either the mother or daughter. Thus, we find that NPCs are segregated concomitantly with the NE between mother and daughter cells and that asymmetry in the NPC assembly pathway is minimal for these components.

In contrast to the scaffold nups, the FG-nup Nsp1-GFP did not display a symmetrical distribution. First, although low levels of NE fluorescence could be visualized in the mother and daughter, a discrete Nsp1-GFP focus was visualized in the daughter at the cell cortex (Fig. 1 F, arrowheads). As anaphase progressed, the focus moved from the cortex and integrated into the NE (Fig. 1 F and Video 1). Consistent with these observations, the calculated tf_d/tf_m of the GFP fluorescence remained at ~0.2 for the first three stages of anaphase, but by cytokinesis the ratio reached ~0.7, as exhibited by old and new ratios of all nups (Fig. 1, F1). To rule out that this

pool of Nsp1 resulted from an aggregation or instability of the GFP-tagged Nsp1, we confirmed that the cytoplasmic Nsp1-GFP accumulation could be reproduced with monomeric GFP (Fig. S2 A), and there was no change in protein levels or stability of Nsp1-GFP compared to untagged Nsp1 by Western blotting (Fig. S2 B). Further, as shown in Fig. S2 C, we could observe bud-localized foci of untagged Nsp1 by immunofluorescence using specific anti-Nsp1 antibodies. In addition, we affinity purified Nsp1-GFP and confirmed that all established interacting partners including Nup49, Nup57, Nic96, Nup159, Dyn2, and Nup82 (Nehrbass et al., 1990; Grandi et al., 1993, 1995; Zabel et al., 1996; Schlaich et al., 1997; Bailer et al., 2001; Stelter et al., 2007) were specifically enriched compared to controls (Fig. S2 D). Last, the Nsp1 fusion proteins generated in this study support viability (Fig. 2 B). Collectively, these data support the finding that the Nsp1-GFP foci represent a previously undiscovered pool of Nsp1 localized to daughter cells before completion of anaphase.

"Anchor-away" of newly synthesized cytoplasmic nups

To directly query the function of this bud-localized pool of Nsp1, we needed an experimental system capable of rapid and specific abrogation of the function of a newly synthesized cytoplasmic pool of nups (which we term nup$_{CYT}$) without affecting

the pool assembled into NPCs (nup_{NPC}). We adopted the "anchor-away" system (Haruki et al., 2008), which exploits the conditional high-affinity dimerization of the FRB and FKBP12 protein domains in the presence of the drug rapamycin (Fig. 2 A). By expressing nups as an FRB fusion, we selectively recruit their newly synthesized nup_{CYT} pools to an abundant plasma membrane trap (Pma1-FKBP12; Fig. 2 A). Growth of Nup-FRB fusion–containing strains on medium with carrier alone (DMSO) showed that the FRB moiety does not appreciably influence their fitness (Fig. 2 B), whereas the addition of rapamycin led to growth arrest, which is consistent with the trapping of essential proteins (Figs. 2 B and S3). Further, plasmid-expressed *NSP1* and *NIC96* were able to suppress rapamycin-induced growth inhibition, ensuring that nup trapping did not act as a dominant-negative (Fig. 2 B). As expected, we observed an accumulation of all tested Nup-FRB-GFP fusions at the plasma membrane after incubation in the presence of rapamycin (Fig. 2 C).

To test whether our trap was specific to nup_{CYT} over nup_{NPC}, we incubated strains expressing Nup-FRB-GFP fusions in the presence of rapamycin and cycloheximide (to inhibit protein synthesis). Under these conditions, the Nup-FRB-GFP plasma membrane pool was completely absent, and nup_{NPC} was unaffected (Fig. 2 C). These data are consistent with the interpretation that the plasma membrane pool is made up exclusively of Nup-FRB-GFP$_{CYT}$. Thus, this system is capable of specifically inhibiting nup_{CYT} without affecting nup_{NPC}.

Trapping of the Nsp1 complex reduces NPC number in daughter cells

Since the Nsp1$_{CYT}$ foci are newly synthesized and appear to be integrated into the NE at the end of anaphase (Fig. 1 F), we reasoned that they might represent NPC assembly intermediates. We therefore examined how trapping of Nsp1-FRB-GFP$_{CYT}$ impacted the relative levels of NPCs in mother and daughter cells after anaphase completion. Because there is little turnover of $nups_{NPC}$ (Fig. 2 C), we assume that Nup-FRB-GFP$_{NPC}$ represents NPCs; we localized Nup170-mCherry in the same cells as an independent NPC marker. Nsp1-FRB-GFP–expressing cells were grown to mid-log phase, incubated in the presence of rapamycin or carrier alone (DMSO), and imaged over one to two cell cycles (Fig. 3 A). Strikingly, the trapping of Nsp1-FRB-GFP$_{CYT}$ resulted in a dramatic reduction in the levels of Nsp1-FRB-GFP$_{NPC}$ in daughter cells after mitosis, while also affecting (although to a lesser extent) the daughter levels of Nup170-mCherry (Fig. 3B). When expressed as a tf_d/tf_m ratio, we observed a 72% reduction in daughter levels of Nsp1-FRB-GFP$_{NPC}$ from an average tf_d/tf_m of 0.57 in DMSO-treated cells compared to 0.16 in trapped cells (Fig. 3 C). This change in NPC levels could not be explained by the relatively modest (34%) change in nuclear size observed upon trapping Nsp1-FRB-GFP$_{CYT}$ (Fig. S4). Similar experiments were performed with additional members of the Nsp1 complex including Nup49-FRB-GFP, Nup57-FRB-GFP, and Nic96-FRB-GFP. In these cells, the tf_d/tf_m ratios were also significantly reduced in the presence of rapamycin (Fig. 3 C). Because we did not observe a restriction of NPC inheritance under wild-type conditions (Fig. 1), these data

suggest that there is a specific inhibition of the transmission of NPCs upon sequestering newly synthesized, cytoplasmic components of the Nsp1 complex.
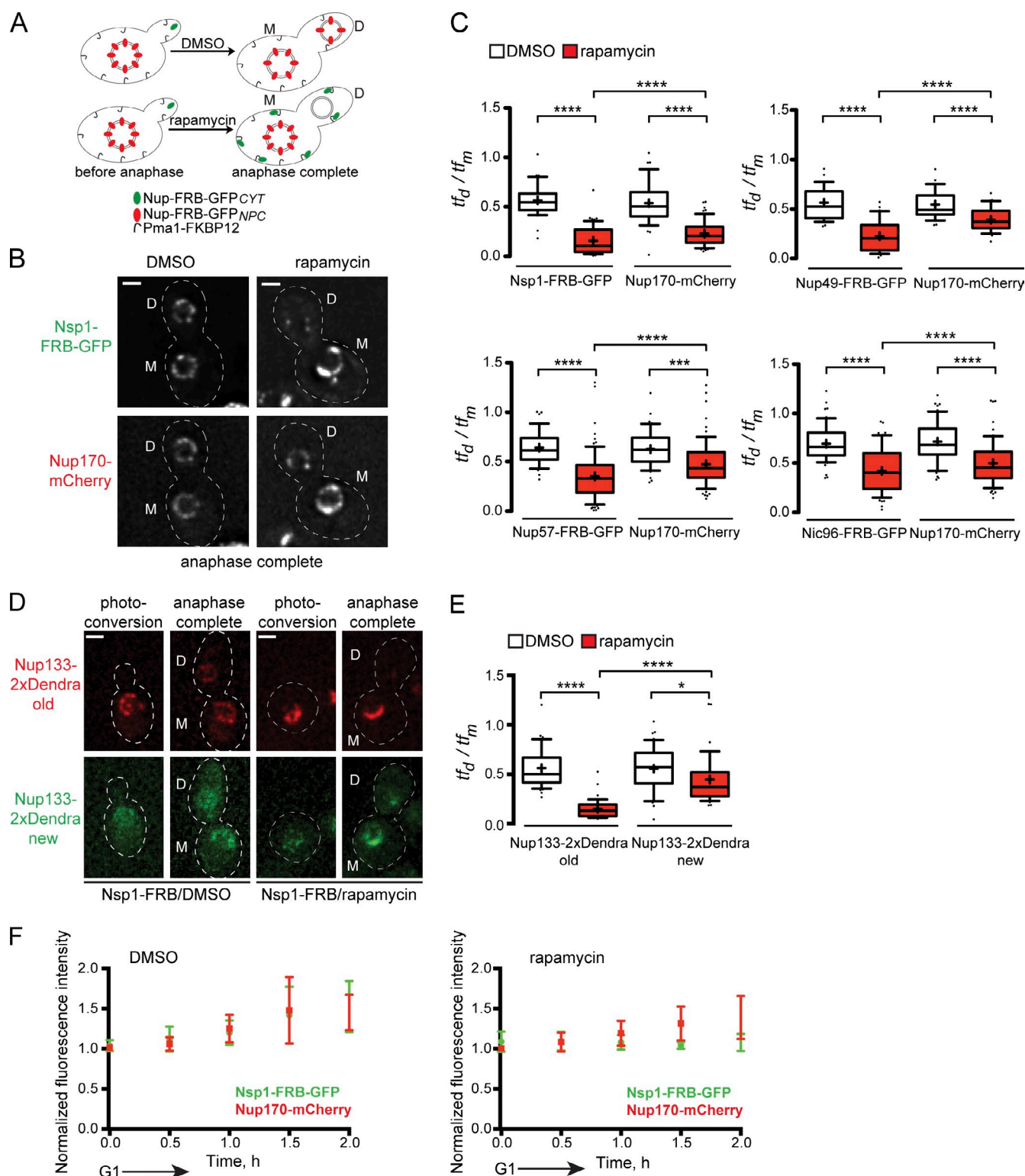
To further test if trapping of the Nsp1 complex leads to the specific loss of the transmission of NPCs to daughter cells, we localized an assembled and stable component of the NPC, Nup133, tagged with the photoconvertible Dendra fluorescent protein in an Nsp1-FRB–containing strain. We irreversibly photoconverted the majority of Dendra from its green to red form in G1/S-phase cells such that any remaining Nup133 protomers would complete assembly into NPCs before anaphase (Fig. 3 D; "photoconversion"). We then tracked the red fluorescent (assembled/old) NPCs through the cell cycle in the presence of either DMSO or rapamycin. Strikingly, rapamycin treatment resulted in a severe loss of the inheritance of old Nup133-Dendra (Fig. 3 D), which is reflected in the change of tf_d/tf_m ratios from 0.56 to 0.15 (Fig. 3 E). These data support the conclusion that NPCs are not inherited when Nsp1$_{CYT}$ is inhibited.

Interestingly, we observed a weak accumulation of the green "new" Nup133-Dendra in daughter cells (Fig. 3 D) shown by the difference in the mean red and green tf_d/tf_m ratios (0.15 and 0.44, respectively; Fig. 3 E), which suggests that NPC assembly continues after Nsp1$_{CYT}$ is trapped. To test this, we monitored the levels of Nsp1-FRB-GFP$_{NPC}$ and Nup170-mCherry in cells progressing from G1 to G2/M. In DMSO-treated cells, both GFP and mCherry fluorescence increased with similar kinetics, which we interpret to represent de novo NPC assembly (Fig. 3 F). In contrast, in rapamycin-treated cells, Nsp1-FRB-GFP levels remain constant while Nup170-mCherry increases, perhaps reflecting the accumulation of an NPC assembly intermediate (Fig. 3 F). Consistent with this idea, the tf_d/tf_m ratios of Nup170-mCherry were significantly higher than the tf_d/tf_m ratios of their Nsp1 complex FRB-GFP$_{NPC}$ partners (Fig. 3 C). Thus, the Nup170-mCherry–containing NPC assembly intermediates might either be transmitted or assembled in the daughter when the Nsp1 complex is trapped.

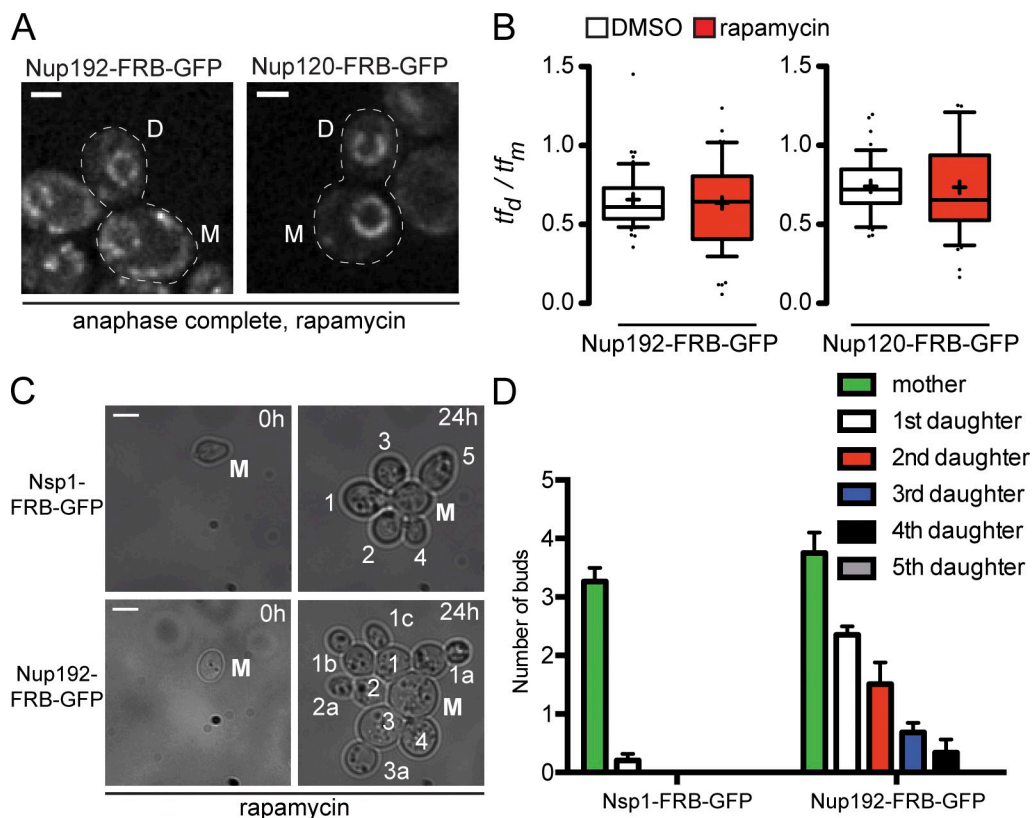### NPC assembly blocks do not affect NPC inheritance

To test if the mechanism of NPC transmission required de novo NPC assembly, we generated a strain expressing the essential inner ring nup Nup192 as a FRB-GFP fusion (Fig. S3). Because the inner ring complex is thought to assemble upstream of the Nsp1 complex (Kosova et al., 1999; Gomez-Ospina et al., 2000; Makio et al., 2009; Onischenko et al., 2009), trapping of Nup192 allowed us to ask whether inhibition of NPC assembly influences the transmission of NPCs. As shown in Fig. 4 A, under rapamycin and DMSO conditions the relative levels of Nup192-FRB-GFP$_{NPC}$ between mother and daughter cells did not change (tf_d/tf_m ratios of ∼0.6; Fig. 4 B), which suggests that compromised NPC assembly does not influence the mechanism of NPC transmission. Similar results were obtained upon trapping the outer ring component Nup120 (Fig. 4, A and B).

If there is a mechanism to specifically drive NPC transmission to daughter cells, we hypothesized that inhibition of this pathway would lead to daughter-specific phenotypes distinct from those in NPC assembly mutants. To test this idea, we

Figure 3. **Trapping of newly synthesized components of the Nsp1 complex inhibits NPC inheritance.** (A) Schematic of the experimental design where anchor-away (see Fig. 2) strains expressing Nup-FRB-GFP fusions were grown to mid-log phase and treated with DMSO or rapamycin (to trap Nup-FRB-GFP$_{CYT}$). Unbudded cells were imaged through one or two cell cycles (~4 h). Quantification of Nup-FRB-GFP$_{NPC}$ was performed at a time point directly after anaphase is completed in mother (M) and daughter (D) cells. (B) Deconvolved fluorescent images showing the distribution of Nsp1-FRB-GFP and Nup170-mCherry (CPL1229) in a middle z plane of cells treated with DMSO or rapamycin after anaphase. Pixels in the GFP channel have been digitally saturated to aid in the visualization of the daughter NE. Cell boundaries are denoted by the outlines. Bar, 2 μm. (C) In each of the indicated Nup-FRB-GFP/Nup170-mCherry–expressing strains (CPL1229, PCCPL510, PCCPL511, and PCCPL293), the *tf* of the GFP and mCherry fluorescence of daughter (*tf$_d$*) and mother (*tf$_m$*) NEs was measured after completion of anaphase under DMSO- or rapamycin-treated conditions. $30 \le n \le 75$. A ratio of *tf$_d$/tf$_m$* was plotted for individual cells in a box plot: boxes are the 25th to 75th percentiles and whiskers are the 10th and 90th percentiles. Outliers are shown as individual points. The mean is indicated by "+." Significance was assessed using the Student's *t* test. ***, P = 0.0003; ****, P < 0.0001. (D) Small-budded

Figure 4. NPC inheritance does not depend on de novo NPC assembly but is required for daughter viability. (A) Deconvolved image of a middle z plane showing Nup192-FRB-GFP (PCCPL528) or Nup120-FRB-GFP (WZCPL5) after completion of anaphase in the presence of rapamycin. M and D, mother and daughter, respectively. Bars, 2 µm. (B) Plot of tf_d/tf_m for Nup192-FRB-GFP and Nup120-FRB-GFP as in Fig. 3. $42 \leq n \leq 55$. (C) Single mother (M) cells expressing Nsp1-FRB-GFP (PCCPL487) or Nup192-FRB-GFP (PCCPL552) were grown in a microfluidic chamber perfused with rapamycin for 24 h. Each daughter was assigned a number (starting with 1) and their daughters assigned the same number followed by a letter to denote their parentage and order of appearance (starting with "a"). Bars, 5 µm. (D) Quantification of C where the average number of buds from mother and daughter cells is plotted. 29 and 32 mother cells (from two independent experiments) were analyzed for PCCPL487 and PCCPL552 strains, respectively. Error bars indicate standard deviation from the mean.
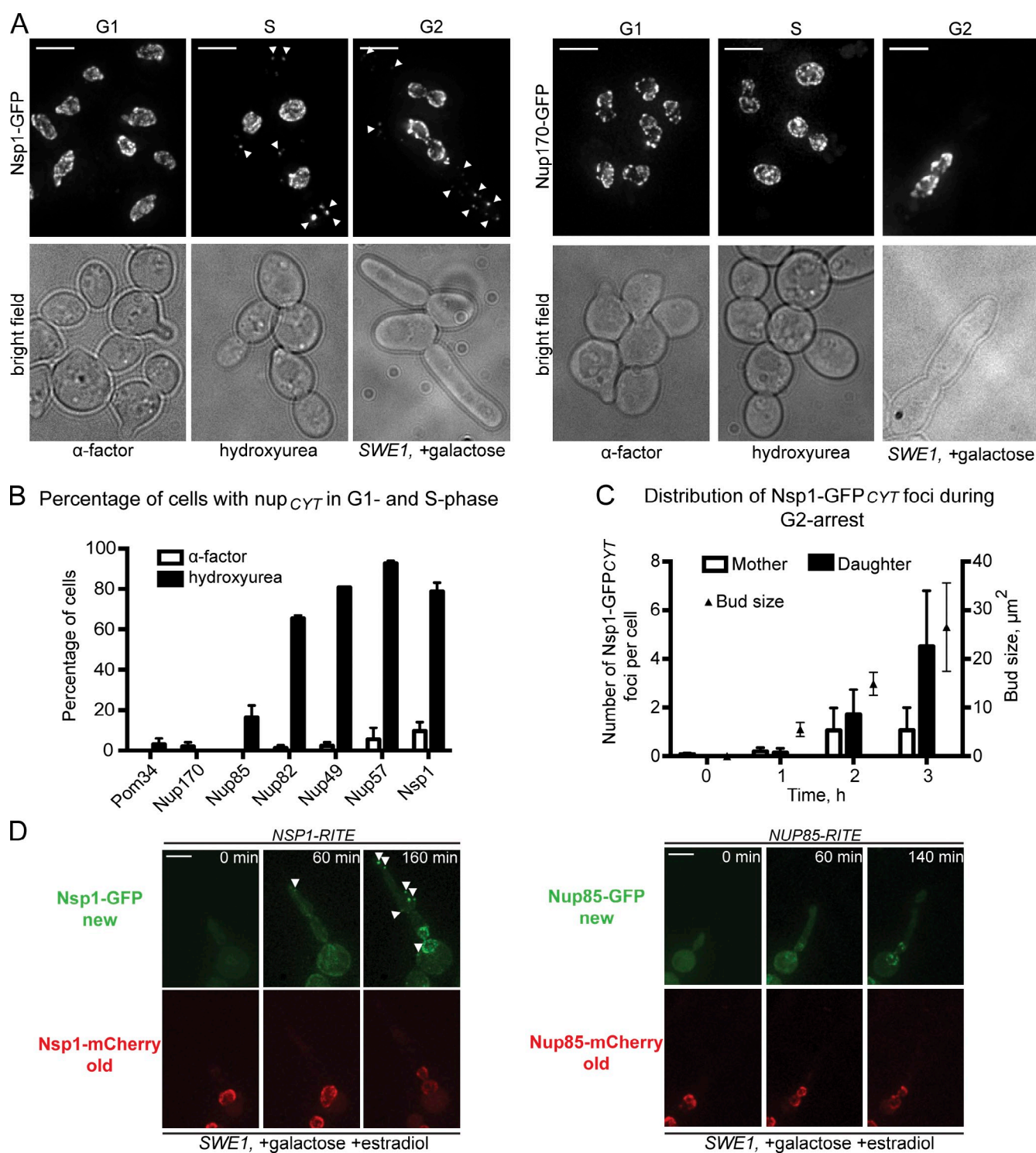
grew Nsp1-FRB-GFP– and Nup192-FRB-GFP–containing cells in the presence of rapamycin. In both cases, the cells ceased to grow after ∼24 h and were vacuolated, suggesting a loss of viability (Fig. 4 C). Interestingly, while the initial Nsp1-FRB-GFP mother cell (time 0) was able to give rise to multiple progeny (mean of 3.2; Fig. 4 D), almost all of its daughters failed to bud, which indicates a daughter-specific growth arrest. In contrast, daughter cells from the Nup192-FRB-GFP mother continued to bud with a frequency reflecting the order by which they were born; the first daughter budded an average of 2.3 times, whereas the fifth daughter never budded (Fig. 4 D). These data are consistent with the interpretation that the transmission of NPCs to daughters results in their dilution after each division, leading to a loss of viability of all cells. We suggest that the loss of viability of the Nsp1-GFP-FRB mother cell is not due to the retention

of NPCs, rather it is likely the result of the assembly of NPCs lacking Nsp1, which would ultimately compromise nuclear–cytoplasmic compartmentalization.

Specific bud localization of components of the Nsp1 complex

To unravel the mechanism of NPC transmission, we performed experiments to understand the production, dynamics, and localization of $Nsp1_{CYT}$ foci. We first investigated whether $Nsp1_{CYT}$ production is cell cycle stage dependent. We localized Nsp1-GFP after blocking cell cycle progression in G1, S, or G2 using α-factor, hydroxyurea, and *SWE1* overexpression, respectively (Fig. 5 A). In G1-arrested cells, no Nsp1-GFP accumulated within cytoplasmic structures. In contrast, upon S and G2 arrests, Nsp1-GFP could be visualized within cytoplasmic foci

cells expressing Nsp1-FRB and Nup133-2xDendra (CPL1231) were treated with DMSO or rapamycin. Nup133-2xDendra was photoconverted to its red form (photoconversion) and allowed to progress through anaphase. The fluorescence images are a middle focal plane from a deconvolved z series in red (old) and green (new) channels. Cell boundaries are denoted by the outlines. Bar, 2 µm. (E) tf_d/tf_m for both red and green fluorescence (and statistics) are plotted as in C. $36 \leq n \leq 47$. *, $P < 0.05$; ****, $P < 0.0001$. (F) CPL1229 expressing Nsp1-FRB-GFP and Nup170-mCherry was treated with DMSO or rapamycin. G1 cells were imaged until anaphase (2 h), and *tf* was measured for both GFP and mCherry every 30 min. *tf* measurements were normalized to the minimum value in each time series and plotted against time (h). Error bars are the standard deviation from the mean. $n = 6$.

Figure 5. **The Nsp1 complex has a cytoplasmic pool localized to the daughter bud.** (A) Fluorescence micrographs (and bright field) of Nsp1-GFP– and Nup170-GFP–expressing cells (CPL1234, BWCPL437, PCCPL423, and PCCPL409) arrested in G1, S, or G2 phase with α-factor–, hydroxyurea-, or galactose-induced overexpression of *SWE1*, respectively. To visualize cytoplasmic foci, we show maximum-intensity projections of a deconvolved z series where 0.4% of pixels have been digitally saturated. Bars, 5 µm. (B) Plot showing the percentage of cells where the indicated nups were found in cytoplasmic foci in α-factor– or hydroxyurea-arrested cells. $90 \leq n \leq 190$. Error bars indicate standard error of the mean. (C) Plot showing the number of Nsp1-GFP$_{CYT}$ foci and their distribution in daughter buds and mother cells during 3 h of a G2 arrest. At the indicated times, >100 cells were scored. Error bars indicate standard deviations from the mean. Bud size is the surface area of the bud (μm^2). (D) *NSP1*-(PCCPL506)– and *NUP85-RITE* (PCCPL523)–containing strains were grown in the presence of galactose (to induce a G2 arrest) and estradiol and imaged over several hours (see Videos 2 and 3). Fluorescence micrographs (maximum-intensity projections of a deconvolved z series) of the GFP and mCherry forms of Nsp1 and Nup85 are shown at the indicated time points. Note the specific appearance of Nsp1-GFP "new" (arrowheads) in the elongated bud. Bars, 5 µm.

(Fig. 5 A, arrowheads). Consistent with our RITE experiments, these foci were specific for the Nsp1 complex, with Nsp1, Nup82, Nup49, and Nup57 appearing in a cytoplasmic pool in ∼80% of S-phase–arrested cells (Fig. 5 B), whereas analogous structures were not observed with Nup170-GFP or Pom34-GFP (Fig. 5, A and B). We observed Nup85-GFP in cytoplasmic foci in 16% of cells, but our inability to similarly localize either membrane (Pom34) or inner ring (Nup170) nups argues against the idea that these cytoplasmic foci are annulate lamellae (Kessel, 1992).

Interestingly, the distribution of the $Nsp1_{CYT}$ foci was biased toward the daughter bud (Fig. 5 C). This bud bias was most evident in cells arrested in G2 in which the polarized/apical growth pathway is hyperactivated (Sia et al., 1998; McMillan et al., 1999); under these conditions the number of foci increased with bud size, with greater numbers found in the bud (Fig. 5 C). These data suggest an active targeting or retention mechanism for $Nsp1_{CYT}$ in daughter cells. To further establish that this bud pool is distinct from $Nsp1_{NPC}$, we arrested cells containing the Nsp1-RITE cassette in G2 in the presence of estradiol. In these cells, the first "new" Nsp1-GFP signal appeared as a focus in the daughter bud (Fig. 5 D, arrowheads; and Video 2). As we prolonged the arrest, additional $Nsp1-GFP_{CYT}$ foci accumulated in the bud concomitantly with a NE pool. We did not observe any "old" Nsp1-mCherry in the cytoplasm, nor did we detect a similar bud-localized accumulation of "new" or "old" Nup85 (Fig. 5 D and Video 3). These data further support the existence of two pools of Nsp1: one that is assembled into NPCs ($Nsp1_{NPC}$) and another that is actively targeted and/or retained in the daughter cell ($Nsp1_{CYT}$).

$Nsp1_{CYT}$ foci localize to ER connected to the mother NE

We felt that understanding the role of Nsp1 in NPC transmission required defining how $Nsp1_{CYT}$ is localized to the bud. We therefore tested colocalization of $Nsp1-GFP_{CYT}$ with components of the polarity apparatus and organelles actively transported to daughters, like ER. For these experiments, we delayed cells before anaphase using a temperature-sensitive *cdc6-1* allele (Liang et al., 1995). By arresting *cdc6-1* cells in G2/M at the nonpermissive temperature and then imaging them under permissive conditions, we can exert consistent control over the production of the $Nsp1-GFP_{CYT}$ foci. Using this strategy, we failed to observe colocalization between $Nsp1-GFP_{CYT}$ and several bud-directed factors including Kar9 (Fig. 6 A), Myo2, Abp140 (Yang and Pon, 2002), Abp1 (Wesp et al., 1997; Goode et al., 2001; Fig. S5), or Bud6 (unpublished data; Amberg et al., 2005). We did observe a transient colocalization of Nsp1-GFP-$_{CYT}$ with the exocyst subunit, Exo70 (Fig. 6 B). Interestingly, mammalian Nsp1/Nup62 interacts with Exo70 at the leading edge of migrating cells (Hubert et al., 2009; Béaslas et al., 2012), raising the possibility that this interaction is conserved, even if transient.

In contrast to the fleeting Nsp1-Exo70 colocalization, we observed a stable association between $Nsp1-GFP_{CYT}$ foci and ER (visualized with HDEL-DsRed; Fig. 6 C). For example, in Fig. 6 D, an $Nsp1-GFP_{CYT}$ focus (arrowhead) remains associated
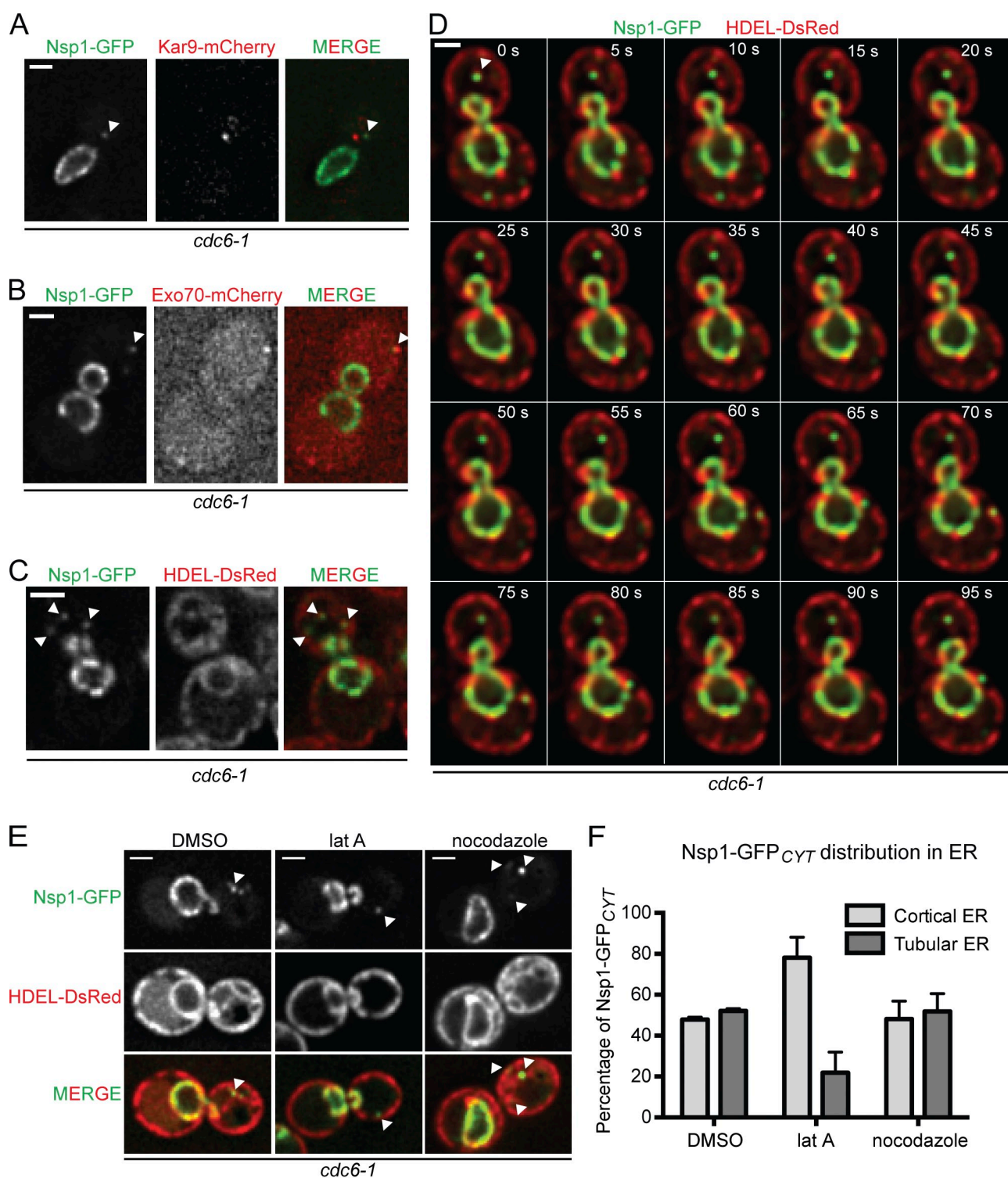
with an ER tubule that extends from the mother NE to the daughter cortex for >95 s (Video 4). Moreover, we colocalized $Nsp1-GFP_{CYT}$ with a bolus of ER originating from the mother NE and traveling to the daughter cortex over 15 min (Fig. S5 B). Because ER morphology in yeast requires an intact actin cytoskeleton (Prinz et al., 2000; Fehrenbacher et al., 2002), we tested the association of $Nsp1_{CYT}$ with ER after disrupting actin filaments by treatment with latrunculin A. Under this condition, we observed a reduction in tubular ER in the bud (Fig. 6 E), and the majority of $Nsp1-GFP_{CYT}$ foci localized to the cell cortex, presumably with cortical ER (Fig. 6, E and F). No effect on ER structure, or $Nsp1_{CYT}$ distribution, was observed after disrupting the spindle with nocodazole (Fig. 6, E and F).

The association of $Nsp1_{CYT}$ with ER was further confirmed by immuno-EM using anti-Nsp1 antibody staining followed by gold-labeled secondary antibodies on ultrathin sections. The anti-Nsp1 antibody was highly specific, as quantification of gold particles at the nucleus showed that >93% were at the NE (Fig. 7 A). Further, NPCs were often decorated with two or more gold particles (Fig. 7 B). Outside the nucleus, we observed gold particles in the cytoplasm and on membranes (Fig. 7 C, arrowheads). We assessed that 40% of the gold particles were associated with membranes that could be morphologically identified as either internal ER (Fig. 7, A and D) or cortical ER (Fig. 7, E and F). Collectively, the combination of our fluorescence and EM data support the conclusion that $Nsp1_{CYT}$ associates with ER, which likely plays a role in its localization to the bud.

$Nsp1_{CYT}$ interacts with nucleopodia (NP) and functions in nuclear positioning

The association of $Nsp1_{CYT}$ with ER extending from the mother NE and the potential interaction with Exo70 prompted us to investigate whether Nsp1's role in NPC transmission might function alongside a recently described nuclear positioning pathway (Kirchenbauer and Liakopoulos, 2013). In this pathway, ER tubules connect the mother NE to the daughter cortex through the exocyst complex (of which Exo70 is a member; Fig. 8 A). This interaction is thought to help drive the formation of NP; dynamic bud extensions of the mother NE are proposed to help maintain nuclear position at the bud neck (Kirchenbauer and Liakopoulos, 2013; Fig. 8 A). We first tested whether the $Nsp1_{CYT}$ foci might be physically connected to NP by time-lapse imaging of *cdc6-1* cells. After release from the *cdc6-1* arrest, NP are observed as the mother NE vectorially extends into the bud and dynamically retracts throughout the ∼1 h time lapse shown in Fig. 8 B (see Video 5 and also Videos 6 and 7). Remarkably, NP move toward a bud-localized $Nsp1-GFP_{CYT}$ focus (Fig. 8 B, arrowheads), appear to "kiss" it, and retract to the mother. This occurs multiple times before the NE absorbs the focus at the end of the time lapse. NP in strains expressing Nup170-GFP do not extend substantially beyond the bud neck, and the NE signal is continuous between mother and bud portions (Fig. 8 B, right; and Video 8).

The interaction between $Nsp1_{CYT}$ and NP prompted us to investigate whether trapping of $Nsp1-FRB_{CYT}$ might, in addition to affecting NPC transmission, impact nuclear positioning at

Figure 6.   **Nsp1-GFP$_{CYT}$ foci interact with ER in the daughter cell.** In all images shown, *cdc6-1* cells were arrested in G2/M for 3 h at 34°C and then imaged at RT. (A–C) Deconvolved fluorescence micrographs of one z section of *cdc6-1* cells expressing Nsp1-GFP and either Kar9-mCherry (PCCPL535), Exo70-mCherry (PCCPL532), or HDEL-DsRed (PCCPL533). Green and red channels are shown in addition to the merge. Arrowheads point to Nsp1-GFP$_{CYT}$ foci. (D) A time-lapse series (Δt = 5 s) of PCCPL533 cells. Each time point is a merge of Nsp1-GFP and HDEL-DsRed images from one z plane. Arrowheads point to a Nsp1-GFP$_{CYT}$ focus (Video 4). (E) PCCPL533 cells were treated with latrunculin A (lat A), nocodazole, or DMSO. Deconvolved micrographs from one z section of a representative cell are shown (green, red, and merged images). Nsp1-GFP$_{CYT}$ foci are indicated by arrowheads. (F) Quantification of E showing the distribution of Nsp1-GFP$_{CYT}$ between the cortical and tubular ER under the indicated conditions. 58 ≤ n ≤ 71. Bars, 2 µm.

the bud neck. To test this idea, we treated cells expressing either Nsp1-FRB-GFP or Nup192-FRB-GFP with rapamycin and monitored nuclear position in small or unbudded cells as they

moved through the cell cycle. Hmg1-mCherry was used to visualize the NE (Fig. 8 C). As expected, under DMSO-treated conditions, 94% of nuclei moved to the bud neck before anaphase
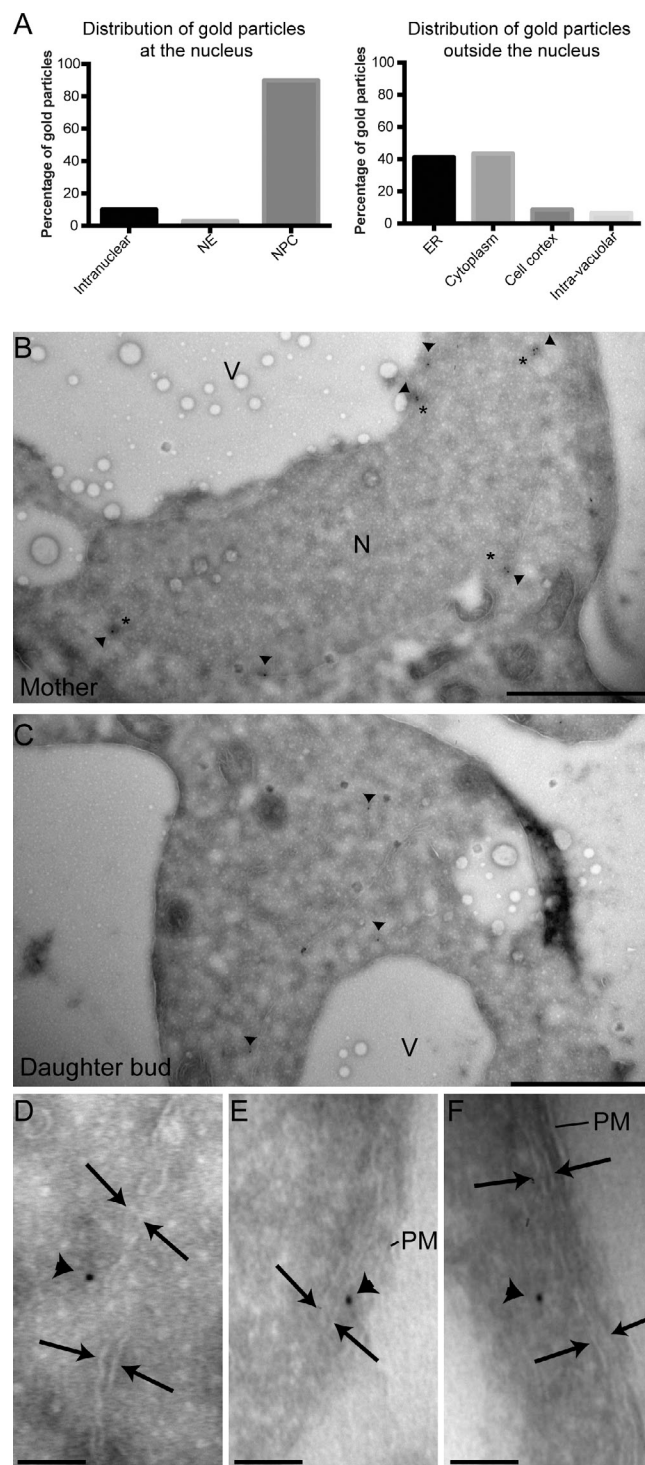
and 98% of nuclei were properly positioned when Nup192-FRB-GFP was trapped (Fig. 8, C and D). In contrast, in 25% of rapamycin-treated Nsp1-FRB-GFP cells, the nuclei were found at a distal location to the neck, which supports the conclusion that the inhibition of Nsp1$_{CYT}$ impacted the ability of cells to position their nuclei correctly (Fig. 8, C and D).

Nsp1$_{CYT}$ distribution and daughter NPC density require *MYO2*

Our observations that trapping of Nsp1$_{CYT}$ impacts NPC inheritance and nuclear positioning suggested that these two processes might be coupled. To explore this idea, we investigated Nsp1$_{CYT}$ distribution and NPC inheritance in strains with mutations in the canonical myosin- and dynein-dependent nuclear positioning pathways. We tested the distribution of Nsp1-GFP by arresting strains containing temperature-sensitive alleles of *MYO2* or knockouts of dynein heavy (*DYN1*) and light (*DYN2*) chain in S phase (Fig. 9 A). Remarkably, in the *myo2* strains, we observed a substantial redistribution of the Nsp1-GFP$_{CYT}$ foci from a predominantly bud-biased distribution to one that was unbiased or biased to the mother (Fig. 9, A and B). In contrast, Nsp1-GFP$_{CYT}$ was not affected in *dyn1Δ*, *dyn2Δ*, and *myo4Δ* strains (Fig. 9, A and B). These data predict that NPC transmission requires Myo2 function. To test this idea, we calculated the mean fluorescence intensity (*mfi*) of a scaffold component of the NPC (Nup85-GFP) at the NE as an indirect measure of NPC density and expressed this as a daughter/mother ratio (mfi_d/mfi_m). Consistent with an active mechanism to deliver NPCs to the daughter, in wild-type cells the average mfi_d/mfi_m ratio was >1 (1.20), which suggests a higher density of NPCs in daughter cells compared to mother cells after anaphase completion (Fig. 9, C and D). These results were mirrored in *dyn1Δ*, *dyn2Δ*, and *myo4Δ* cells. In contrast, in *myo2-14* cells the mean mfi_d/mfi_m was 0.94 (Fig. 9 D), a significant difference (P < 0.0001) from wild-type cells. Collectively, these data provide support to the conclusion that NPC transmission to the daughter cell specifically depends on the Myo2-dependent localization of Nsp1.
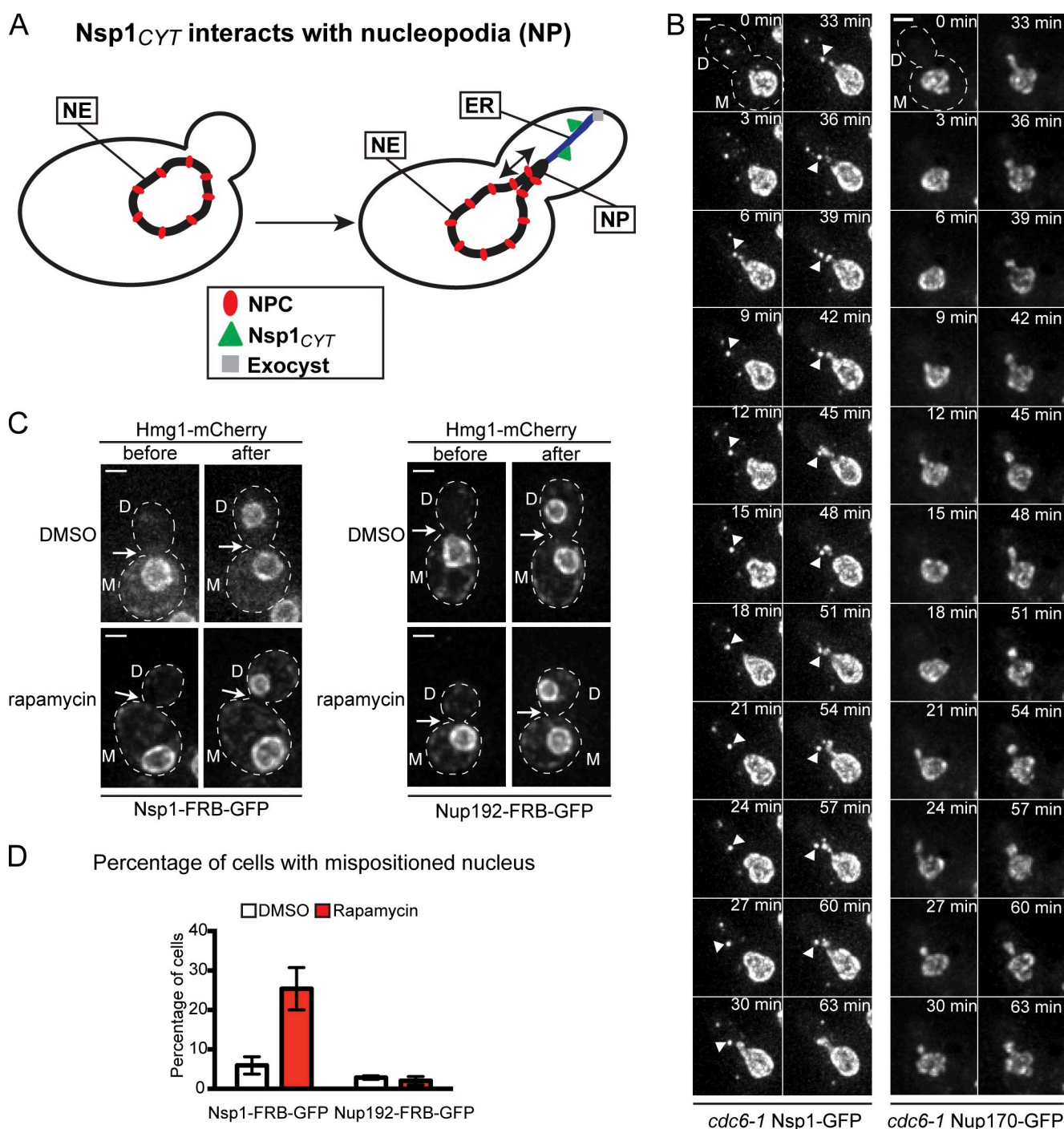
Discussion

We have uncovered a mechanism that controls the inheritance of NPCs in budding yeast based on a bud-directed pool of the Nsp1 complex. Such a mechanism helps explain why daughter cells have a higher density of NPCs (Fig. 9, C and D) and are enriched in "old" nups (Khmelinskii et al., 2012). We conclude that inheriting, as opposed to assembling, NPCs provides the cell the most efficient means to ensure daughter viability. Consistent with this idea, newly synthesized components of the scaffold of the NPC show no preference for the mother or daughter side of the anaphase NE, which argues against a daughter-specific NPC assembly mechanism (Fig. 1). Furthermore, there is no detectable bias in the NPC assembly reaction, as inhibiting assembly by the conditional trapping of either Nup120 or Nup192 did not affect the relative levels of NPCs between mother and daughter cells (Fig. 4, A and B). Indeed, after inhibiting NPC assembly, we and others (Zabel et al., 1996; Makio et al., 2009) show that daughter cells are capable of additional rounds of division,

Figure 7. **Nsp1$_{CYT}$ interacts with ER at high resolution.** *cdc6-1* cells (PCCPL393) were arrested in G2/M phase for 3 h at 34°C, released for 3 h at RT, and then processed for immuno-EM. An anti-Nsp1 antibody followed by a 10 nm gold–conjugated secondary antibody were used to localize Nsp1. (A) Plot of the percentage of gold particles from a single experiment both at (left; n = 71) and outside (right; n = 46) the nucleus in association with the indicated cellular structures. (B and C) EM micrographs of a mother and bud (daughter) of the same cell. N, nucleus; V, vacuole. Asterisks indicate NPCs and arrowheads point to gold particles. Bars, 1 μm. (D–F) High-magnification views of gold particles in association with internal ER (D) and cortical ER (E and F). Arrows delimit the two ER membranes with intervening cistern. Arrowheads point to gold particles. PM, plasma membrane. Bars, 100 nm.
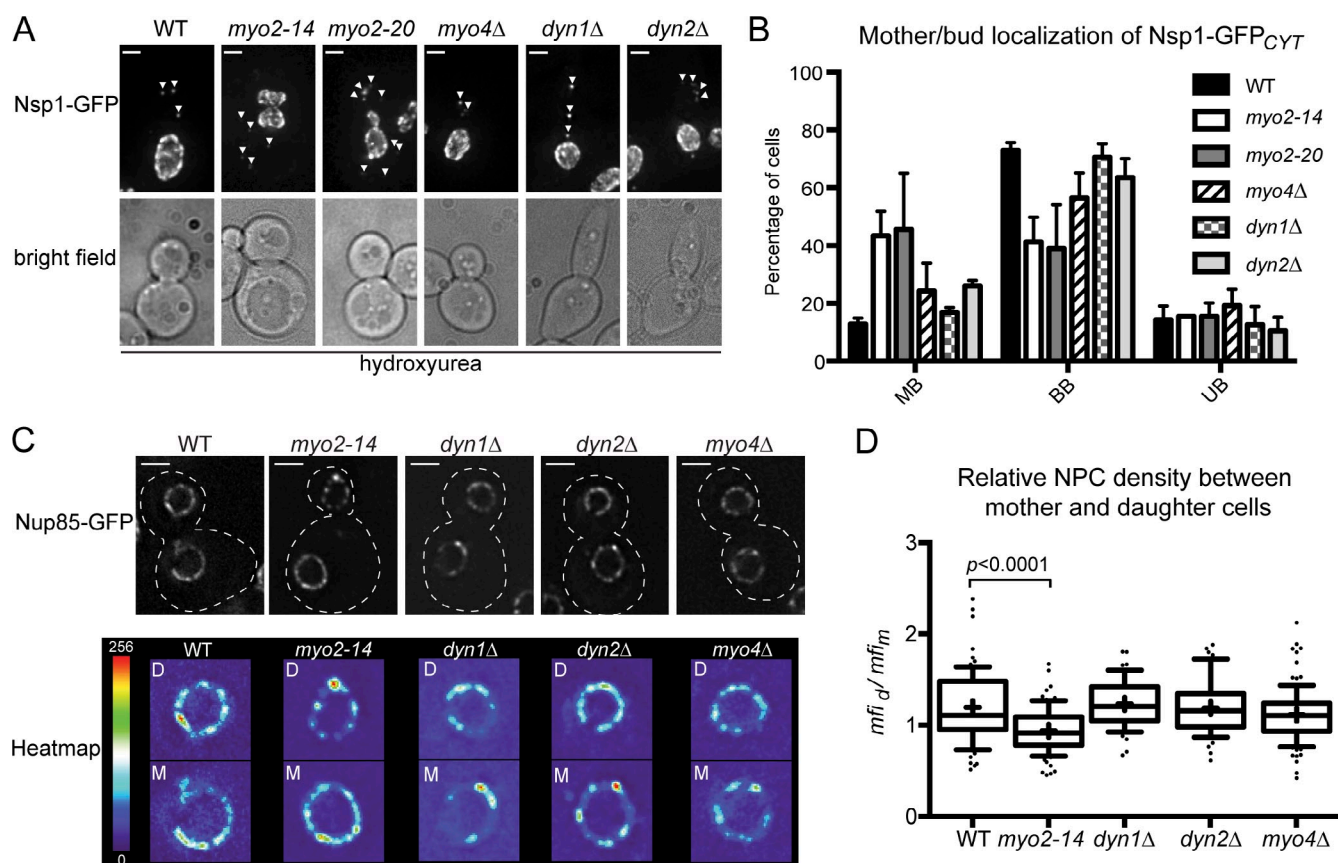
A **Nsp1$_{CYT}$ interacts with nucleopodia (NP)**

B

C Hmg1-mCherry / Nsp1-FRB-GFP ; Hmg1-mCherry / Nup192-FRB-GFP

D Percentage of cells with mispositioned nucleus

cdc6-1 Nsp1-GFP   *cdc6-1* Nup170-GFP

Figure 8. **Nsp1$_{CYT}$ associates with NP and contributes to nuclear positioning.** (A) Schematic of the association of Nsp1$_{CYT}$ with ER tubules that connect the mother NE and daughter cortex through the exocyst complex and contribute to the formation of NP. Red ovals, NPCs; green triangles, Nsp1$_{CYT}$; grey square, exocyst complex. The arrow indicates NP dynamics. (B) Maximum-intensity projections of two time lapses (Δt is 3 min) of a deconvolved z series of fluorescence images. Left panels show the distribution of Nsp1-GFP (PCCPL393; Video 5) and right panels of Nup170-GFP (PCCPL392; Video 8) in *cdc6-1* cells. Arrowheads point to an Nsp1-GFP$_{CYT}$ focus that interacts with NP. Bar, 2 μm. (C) Nsp1-FRB-GFP/Hmg1-mCherry (PCCPL487)– or Nup192-FRB-GFP/Hmg1-mCherry (PCCPL552)–expressing cells were imaged in the presence of DMSO or rapamycin. Individual unbudded cells were followed by time-lapse microscopy until anaphase completion (~2 h). The images shown are maximum-intensity projections of a z series of deconvolved images of cells at the time point just before and after anaphase. M and D, mother and daughter, respectively. The position of the bud neck is indicated by the arrows. Bars, 2 μm. (D) Quantification of C where the percentage of cells showing a mispositioned nucleus is plotted under DMSO and rapamycin conditions. 36 ≤ *n* ≤ 96. Error bars indicate the standard error of the mean.

whereas restriction of NPC transmission results in a daughter-specific growth arrest (Fig. 4, C and D). We suggest that an actively controlled NPC inheritance mechanism might be most relevant when NPC assembly rates cannot keep up with rapid

cell divisions. While the mechanism described here likely varies throughout eukaryotes, the principle that it is more efficient to ensure that components of the NPC are reused as opposed to resynthesized/assembled is likely universal and might help to

Figure 9. **The distribution of Nsp1$_{CYT}$ and the density of daughter NPCs require *MYO2*.** (A) Maximum-intensity projections of a deconvolved z series of images showing the distribution of Nsp1-GFP in wild-type (WT; CPL1234), *myo2-14* (PCCPL317), *myo2-20* (PCCPL316), *dyn1Δ* (PCCPL559), *dyn2Δ* (PCCPL427), and *myo4Δ* (PCCPL365) cells after 3 h of arrest in hydroxyurea at RT. Arrowheads point to Nsp1-GFP$_{CYT}$ foci. Bars, 2 µm. (B) The number and distribution of Nsp1-GFP$_{CYT}$ foci were assessed in the indicated hydroxyurea-arrested cells. For each cell it was determined whether there was a bud-biased (BB), unbiased (UB), or mother-biased (MB) localization in the total number of Nsp1-GFP$_{CYT}$ foci per cell. These numbers were plotted as a percentage of total cells. $40 \leq n \leq 60$. Error bars are standard deviations from the mean. (C) Deconvolved fluorescence micrographs showing a middle z section of WT (BWCPL42), *myo2-14* (PCCPL529), *dyn1Δ* (PCCPL561), *dyn2Δ* (PCCPL445), and *myo4Δ* (PCCPL530) cells expressing Nup85-GFP after anaphase. The bottom panel is a "heatmap" representation of fluorescence intensities normalized to a 1-256 arbitrary scale (legend on the left) of the same mother (M) and daughter (D) cells as in the top panel. Cell boundaries are denoted by outlines. Bars, 2 µm. (D) In a middle z plane of a deconvolved z series, the *mfi* of the NE of a mother and daughter cell were measured and plotted as a ratio (mfi_d/mfi_m) as an indirect readout of relative NPC density. $50 \leq n \leq 98$. Box plot and statistics are as in Fig. 3. P < 0.0001.

explain why nups are so stable (Daigle et al., 2001; D'Angelo et al., 2009; Savas et al., 2012).
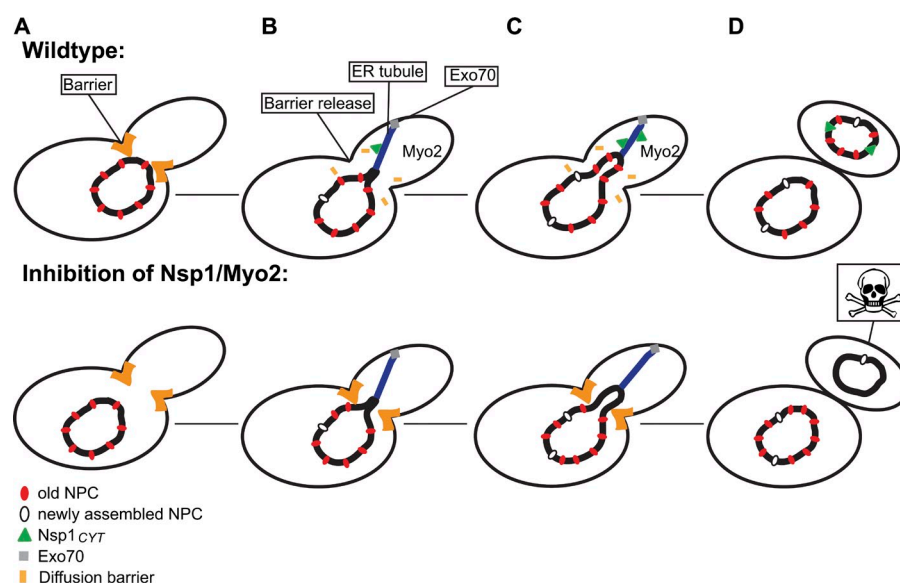
NPC transmission requires the production of an ER-bound pool of Nsp1$_{CYT}$ synthesized before anaphase, likely between S and G2 phase (Fig. 5). Collectively, our data argue that Nsp1$_{CYT}$ acts autonomously from NPCs to carry out this function. First, "old" Nsp1$_{NPC}$ rarely, if ever, exchanges into Nsp1$_{CYT}$ even over many hours of G2 arrest (Fig. 5 D). Consistent with this observation, Nsp1-FRB$_{NPC}$ cannot be trapped at the plasma membrane (Fig. 2). Further, depleting Nsp1$_{CYT}$ has a highly penetrant and rapid effect on daughter viability, whereas a general inhibition of NPC assembly (which would not be predicted to affect Nsp1$_{CYT}$ or NPC transmission; Fig. 4 A) manifests gradually in both mother and daughter cells over several cell cycles (Fig. 4, C and D). Last, the reduction in NPC density in *myo2* daughters more likely reflects a loss of bud targeting of the Nsp1 complex rather than NPC malfunction as nups localize normally to NPCs in these strains (Fig. 9).

There are two general models for how Nsp1$_{CYT}$ might function in promoting the inheritance of NPCs: it helps NPCs either overcome a mother cell retention mechanism similar to that proposed for mitochondria (Yang et al., 1999) or a diffusional barrier at the bud neck (Shcheprova et al., 2008). We favor the model presented in Fig. 10 that invokes the existence of a diffusion barrier since a retention mechanism would be predicted to restrict NPC mobility, which has not been observed (Bucci and Wente, 1997; Belgareh and Doye, 1997). Further, since diffusion barriers would be more likely to impede the passage of large complexes such as NPCs, it predicts that smaller proteins like Hmg1 are able to access daughter cells (Fig. 8 C), as well as putative NPC assembly intermediates (Fig. 3).

In our model, Nsp1$_{CYT}$ moves into the bud by interacting with ER targeted to the daughter (Fig. 10). Interestingly, while the canonical ER inheritance pathway uses Myo4 (Estrada et al., 2003), neither Nsp1$_{CYT}$ distribution nor NPC inheritance are impacted in *myo4Δ* strains (Fig. 9). These data suggest that ER bound by Nsp1$_{CYT}$ may be transmitted to the daughter in a mechanism mediated by the exocyst complex, which subsequently contributes to the formation of NP (Fig. 10; Kirchenbauer and Liakopoulos, 2013). A functional relationship

Figure 10. Model of the mechanism of NPC transmission to daughter cells. (A) In wild-type cells, a diffusion barrier at the bud neck is established (orange). (B) We envision that the delivery of Nsp1$_{CYT}$ (green triangles) to the daughter through a mechanism that requires Myo2 and an association with ER (blue, which bind the daughter cortex through the exocyst complex [grey box]) licenses NPC passage by disrupting the diffusion barrier. (C) Forces applied to the mother NE through NP and/or spindle elongation result in the transmission of NPCs (red ovals). Under conditions in which Nsp1$_{CYT}$ is inhibited or Myo2 function is impaired, the barrier remains intact and restricts the passage of NPCs, leading to the specific loss of viability of daughter cells. De novo NPC assembly continues as indicated by the white ovals.

between NP and Nsp1$_{CYT}$ is consistent with our observation that NP dynamics are directed toward Nsp1$_{CYT}$ (Fig. 8 B). Moreover, both the formation of NP and the localization of Nsp1$_{CYT}$ depend on an intact actin cytoskeleton and Myo2 (Fig. 6, E and F; and 9, A and B) and are required for nuclear positioning at the bud neck (Fig. 8 D). Last, our data point to a potentially conserved interaction between Nsp1 and Exo70, first observed in mammalian tissue culture cells (Fig. 6 B; Hubert et al., 2009).

We propose that the passage of Nsp1$_{CYT}$ through the bud neck licenses NPC transmission during anaphase by either directly (or through an unidentified factor) overcoming the diffusion barrier (Fig. 10). In the absence of Nsp1$_{CYT}$ and/or Myo2 function, the barrier remains intact and NPCs are not able to enter the daughter, leading to a loss of daughter viability (Fig. 10). At this point we can only speculate as to the molecular composition of the bud neck barrier and the signaling factors and/or forces that modulate its function. We envision a mechanism analogous to the recently described ER stress surveillance pathway in which ER stress is signaled through the MAP kinase Slt2 to regulate septin function and impede cortical ER inheritance (Babour et al., 2010). Future experiments will be focused on identifying the internal and/or external inputs that impact Nsp1$_{CYT}$ function that might modulate NPC number.

Materials and methods

Yeast strain generation and growth
All yeast strains used in this study and their derivation are listed in Table S1. ABY530 and ABY534 were gifts from A. Bretscher (Cornell University, Ithaca, NY). YB0044 and PCCPL397 were gifts from B. Stillman (Cold Spring Harbor Laboratory, Cold Spring Harbor, NY), and D. Lew (Duke University, Durham, NC), respectively. Most experiments were performed on yeast grown at 30°C, with the exception of those containing temperature-sensitive alleles (myo2-14, myo2-20, and cdc6-1), which were grown at RT or at 34°C as described in the figure legends. All strains were grown in YP (1% yeast extract and 2% peptone) with 2% dextrose (YPD), 2% raffinose (YPR), or 2% galactose (YPG). Standard yeast manipulations including transformation, tetrad dissection, and PCR-based integration were performed as described in Amberg et al. (2005).

Plasmids
All plasmids and their derivation are listed in Table S2. To generate PLPMR2, the GFP and mRFP genes encoded in pKV015 (a gift from F. van

Leeuwen, Netherlands Cancer Institute, Amsterdam, Netherlands; Verzijlbergen et al., 2010) were sequentially replaced by mCherry and GFP genes, respectively. ORFs encoding NSP1 and NIC96 with their cognate promoters and 3′ UTRs were inserted into pRS416 (Sikorski and Hieter, 1989) to generate PLPC19 and PLPC20. pKW2329 and pKW1358 were gifts from K. Weis (University of California, Berkeley, Berkeley, CA).

Cell cycle arrests
To arrest cells in different phases of the cell cycle, strains were grown to mid-log phase. For G1 arrests, α-factor (Keck Biotechnology Resource Laboratory) was added to a final concentration of 50 µg/ml for 2 h. For S-phase arrest, hydroxyurea (Sigma-Aldrich) was added to the growth medium at a final concentration of 0.2 M for 3 h. G2 arrests were achieved by overexpressing the Swe1 kinase as described in Booher et al. (1993). Strains containing SWE1 behind the control of the GAL1 promoter were grown in YPR to mid-log phase and were shifted to YPG for 3 h. In all cases, cell cycle arrests were confirmed visually by microscopy.

For experiments using strains containing the cdc6-1 allele, cells were grown at RT to mid-log phase and arrested in G2/M by shifting to the nonpermissive temperature of 34°C for 3 h. Cells were then placed on an agarose pad and imaged at RT.

Microscopy
For all imaging experiments, cells were grown to mid-log phase and immobilized on a 1.4% agarose pad containing complete synthetic medium (CSM) with 2% glucose and sealed with VALAP (1:1:1 Vaseline/lanolin/paraffin). All the microscopy experiments were carried out on a wide-field deconvolution microscope (DeltaVision; Applied Precision/GE Healthcare) equipped with a 100×, 1.40 NA objective lens and solid state illumination. The images were acquired using a charge-coupled device (CCD) camera (CoolSNAP HQ²; Photometrics) or an Evolve EMCCD camera (Photometrics). Temperature control was achieved through the enclosure of the microscope within an environmental chamber. In all cases, a z series of images (0.2–0.5-µm sections) were acquired and further processed as described under "Image processing and analysis." Time-lapse series were performed with different time intervals as described in the figure legends.

Immunofluorescence
Cells grown to mid-log phase were collected by centrifugation and fixed in 2% PFA in PBS for 20 min at RT. Cells were subsequently washed in PBS and cell walls were permeabilized by an incubation for 30 min in sorbitol citrate buffer (0.1 M K$_2$HPO$_4$, 0.04 M citric acid, 1.2 M sorbitol, and 0.5 mM MgCl$_2$, pH 6.5) containing 0.02% zymolyase 100T (MP Biomedicals). Cells were washed in sorbitol citrate and transferred to a slide pre-coated with 0.1% poly-L-lysine (Electron Microscopy Sciences). The slide was incubated for 4 min in methanol (−20°C), followed by 4 min in acetone (−20°C). Slides were air dried. The processed cells were then blocked for 20 min with PBS containing 1% BSA and 0.1% Triton X-100 before incubation with an anti-Nsp1 primary antibody (32D6; Abcam) followed by a Alexa Fluor 594–conjugated secondary antibody (Invitrogen).

Image processing and analysis

In all images shown, a z series was deconvolved using the iterative algorithm in softWoRx (version 5.5; Applied Precision). In some cases (indicated in the figure legends), maximum-intensity projections were also generated by softWoRx. Subsequent image processing and analysis was performed using Fiji/ImageJ (Schindelin et al., 2012). To measure tf in daughter and mother cells (tf_d and tf_m), a z stack was sum-projected and background subtracted, and the integrated density of a region of interest (ROI) encompassing the mother or daughter NE was calculated. As an indirect measure of NPC density, we calculated the mfi over an ROI that surrounded only the NE in mother or daughter cells of one middle z plane. To calculate nuclear volume, we measured the ferret diameter of the nucleus through a middle z section. An approximate nuclear volume was calculated by considering that the nucleus was a sphere using the equation $V = 4/3 \, \pi r^3$. All plots and statistical analysis were performed using Prism software (GraphPad Software).

RITE

Nup-RITE–containing strains were grown to mid-log phase in YPD or YPR in the presence of 300 µg/ml hygromycin (Invitrogen) to maintain selection for mCherry expression (Verzijlbergen et al., 2010). Cells were synchronized in G1 with α-factor, washed in YPD or YPR, and released for 1 h in YPD or YPG containing 1 µM estradiol before imaging on an agarose pad.

Anchor-away experiments

For plate-based growth assays, cells were grown overnight and plated in 10-fold serial dilutions on YPD plates containing DMSO or rapamycin (EMD Millipore) at a concentration of 1 µg/ml. Growth was assessed after 48 h at 30°C. For microscopy, mid-log phase cells expressing Nup-FRB-GFP fusions were grown in YPD and placed onto agarose pads containing DMSO, rapamycin (10 µg/ml), or rapamycin and cycloheximide (10 µg/ml; VWR International). Cells expressing Nup133-2xDendra were exposed to seven 0.5-s pulses of UV light to photoconvert Dendra from its green to red fluorescent form. In all experiments, cells that were unbudded or small budded were imaged through at least one cell cycle. For long-term viability/growth assays, cells were transferred to a microfluidic plate (Y04C/CellASIC) within the ONIX microfluidic platform (CellASIC) inserted onto the microscope stage. YPD containing DMSO or rapamycin (10 µg/ml) was perfused into the microfluidic plate at a pressure of 2 psi for 24 h.

Affinity purification of Nsp1-GFP and stable isotope labeling of amino acids in cell culture (SILAC)

For SILAC labeling, lys2Δ (PCCPL314) and lys2Δ NSP1-GFP (PCCPL322) yeast cells were grown in CSM-Lys. Lysine (Sigma-Aldrich) or "heavy" $[^{13}C_6/^{15}N_2]$L-lysine (Cambridge Isotope labs) was added to a final concentration of 30 mg/liter. 100 OD of cells were harvested by centrifugation and resuspended in 500 µl of lysis buffer (150 mM KOAc, 20 mM Hepes, pH 7.4, 10% glycerol, and complete protease inhibitor cocktail [Roche]). 500 µl of zirconia beads (0.1 mm in diameter; BioSpec Products Inc.) were added and cells were lysed using a bead mill (Retsch) running at 30 Hz for 5 min. The beads were removed by centrifugation, and Triton X-100 was added to a final concentration of 1%. After a 30-min incubation at 4°C, the lysate was clarified by a 10-min centrifugation at 1,000 g. Equivalent amounts of PCCPL329 and PCCPL322 lysates were incubated (separately) with GFP-Trap agarose beads (Allele Biotechnology) for 30 min at 4°C. After washing, the beads were combined, and 100 µl of 8 M urea and 50 mM Tris-HCl, pH 7.4, was added. Bound proteins were reduced, alkylated, and digested with the endoproteinase LysC directly on beads. The resulting peptide mixture was removed from the beads, acidified with trifluoroacetic acid, and desalted using stop-and-go extraction tips (StageTips; Rappsilber et al., 2003), which are pipette tips packed with C18 solid phase chromatography resin (3M). Peptides were washed with 0.1% formic acid, eluted with 60 µl of 80% acetonitrile and 0.1% formic acid, and reduced to 5 µl in a speed vacuum centrifuge (Eppendorf). The peptide mixture was subjected to reversed phase chromatography on an Easy nLC system (Thermo Fisher Scientific) using a 50-cm column (New Objective) with an inner diameter of 75 µm, packed in-house with 3 µm C18 resin (Dr. Maisch GmbH). Peptides were eluted with an acetonitrile gradient (5–30%) and directly electrosprayed into a mass spectrometer (LTQ Orbitrap Velos; Thermo Fisher Scientific; Aguilar et al., 2010). Data were acquired with Xcalibur software (version 2.1; Thermo Fisher Scientific) and analyzed with MaxQuant (version 1.2.2.5; Cox and Mann, 2008; Cox et al., 2011) as described previously (Fröhlich et al., 2013). In brief, peak lists were searched against a local database for *S. cerevisiae* (obtained from Saccharomyces Genome Database). Maximum allowed mass deviation for tandem mass spectrometry (MS/MS) peaks and missed cleavages were 20 ppm and 3, respectively. Maximum false discovery rates were 0.01 both on the peptide and on the protein levels. Minimum required peptide length was six residues. Proteins with at least two peptides were considered identified. All calculations and plots were performed with the R software package.

Western blots

Exponentially growing cells were collected by centrifugation and lysed in 0.1 M NaOH for 5 min at RT. The pellet was resuspended in SDS-PAGE sample buffer, and proteins were separated on SDS-PAGE gels and transferred to a nitrocellulose membrane (Bio-Rad Laboratories). We used anti-Nsp1 antibodies (32D6; Abcam) followed by HRP-conjugated secondary antibodies and ECL for detection.

Immuno-EM

Cells were fixed in PBS containing 4% PFA and 0.1% glutaraldehyde for 1 h at RT and embedded in 10% gelatin. They were subsequently infiltrated with 2.3 M sucrose at 4°C overnight and frozen in liquid nitrogen. Thin sections (∼60 nm) were cut with a cryo-ultramicrotome (EM FC6; Leica). Immunolabeling was carried out with the anti-Nsp1 primary antibody for 30 min followed by 10 nm of gold-conjugated secondary antibody for an additional 30 min. Grids were visualized with a transmission electron microscope (Tecnai Biotwin; FEI) at 80 kV. Images were taken using a CCD camera (Morada) fitted with iTEM software (both from Olympus).

Online supplemental material

Fig. S1 demonstrates that Nup-mCherry levels do not increase after RITE is induced. Fig. S2 presents multiple experiments confirming the functionality of the Nsp1-GFP protein. Fig. S3 shows the growth of strains containing Nup-FRB-GFP alleles. Fig. S4 is the quantification of the change of daughter nuclear size upon trapping of Nsp1-FRB-GFP. Fig. S5 examines colocalization between Nsp1-GFP$_{CYT}$ and several components of the polarity apparatus and ER. In Video 1, the production and NE integration of Nsp1-GFP$_{CYT}$ is shown during mitosis. Video 2 is a RITE experiment performed under G2 arrest showing the specific bud localization of only Nsp1-GFP and not Nsp1-mCherry. Video 3 shows the distribution of green and red versions of Nup85-RITE during G2 arrest. In Video 4, the interaction between an Nsp1-GFP$_{CYT}$ focus with an ER tubule is highlighted. Videos 5–7 demonstrate the physical connection between the Nsp1-GFP$_{CYT}$ foci and NP. Video 8 shows the absence of a cytoplasmic pool of Nup170-GFP during NP formation. Online supplemental information is available at http://www.jcb.org/cgi/content/full/jcb.201305115/DC1.

References

Aguilar, P.S., F. Fröhlich, M. Rehman, M. Shales, I. Ulitsky, A. Olivera-Couto, H. Braberg, R. Shamir, P. Walter, M. Mann, et al. 2010. A plasma-membrane E-MAP reveals links of the eisosome with sphingolipid metabolism and endosomal trafficking. *Nat. Struct. Mol. Biol.* 17:901–908. http://dx.doi.org/10.1038/nsmb.1829

Alber, F., S. Dokudovskaya, L.M. Veenhoff, W. Zhang, J. Kipper, D. Devos, A. Suprapto, O. Karni-Schmidt, R. Williams, B.T. Chait, et al. 2007a. The molecular architecture of the nuclear pore complex. *Nature.* 450:695–701. http://dx.doi.org/10.1038/nature06405

Alber, F., S. Dokudovskaya, L.M. Veenhoff, W. Zhang, J. Kipper, D. Devos, A. Suprapto, O. Karni-Schmidt, R. Williams, B.T. Chait, et al. 2007b. Determining the architectures of macromolecular assemblies. *Nature.* 450:683–694. http://dx.doi.org/10.1038/nature06404

Amberg, D.C., D. Burke, and J.N. Strathern. 2005. Methods in Yeast Genetics. Cold Spring Harbor Laboratory Press, Cold Spring Harbor, NY. 230 pp.

Babour, A., A.A. Bicknell, J. Tourtellotte, and M. Niwa. 2010. A surveillance pathway monitors the fitness of the endoplasmic reticulum to control its inheritance. *Cell.* 142:256–269. http://dx.doi.org/10.1016/j.cell.2010.06.006

Bailer, S.M., C. Balduf, J. Katahira, A. Podtelejnikov, C. Rollenhagen, M. Mann, N. Panté, and E. Hurt. 2000. Nup116p associates with the Nup82p-Nsp1p-Nup159p nucleoporin complex. *J. Biol. Chem.* 275:23540–23548. http://dx.doi.org/10.1074/jbc.M001963200

Bailer, S.M., C. Balduf, and E. Hurt. 2001. The Nsp1p carboxy-terminal domain is organized into functionally distinct coiled-coil regions required for assembly of nucleoporin subcomplexes and nucleocytoplasmic transport. *Mol. Cell. Biol.* 21:7944–7955. http://dx.doi.org/10.1128/MCB.21.23.7944-7955.2001

Béaslas, O., T. Vihervaara, J. Li, P.-P. Laurila, D. Yan, and V.M. Olkkonen. 2012. Silencing of OSBP-related protein 8 (ORP8) modifies the macrophage transcriptome, nucleoporin p62 distribution, and migration capacity. *Exp. Cell Res.* 318:1933–1945. http://dx.doi.org/10.1016/j.yexcr.2012.05.026

Belgareh, N., and V. Doye. 1997. Dynamics of nuclear pore distribution in nucleoporin mutant yeast cells. *J. Cell Biol.* 136:747–759. http://dx.doi.org/10.1083/jcb.136.4.747

Belgareh, N., G. Rabut, S.W. Baï, M. van Overbeek, J. Beaudouin, N. Daigle, O.V. Zatsepina, F. Pasteau, V. Labas, M. Fromont-Racine, et al. 2001. An evolutionarily conserved NPC subcomplex, which redistributes in part to kinetochores in mammalian cells. *J. Cell Biol.* 154:1147–1160. http://dx.doi.org/10.1083/jcb.200101081

Bolhy, S., I. Bouhlel, E. Dultz, T. Nayak, M. Zuccolo, X. Gatti, R. Vallee, J. Ellenberg, and V. Doye. 2011. A Nup133-dependent NPC-anchored network tethers centrosomes to the nuclear envelope in prophase. *J. Cell Biol.* 192:855–871. http://dx.doi.org/10.1083/jcb.201007118

Booher, R.N., R.J. Deshaies, and M.W. Kirschner. 1993. Properties of *Saccharomyces cerevisiae* wee1 and its differential regulation of p34CDC28 in response to G1 and G2 cyclins. *EMBO J.* 12:3417–3426.

Bucci, M., and S.R. Wente. 1997. In vivo dynamics of nuclear pore complexes in yeast. *J. Cell Biol.* 136:1185–1199. http://dx.doi.org/10.1083/jcb.136.6.1185

Chadrin, A., B. Hess, M. San Roman, X. Gatti, B. Lombard, D. Loew, Y. Barral, B. Palancade, and V. Doye. 2010. Pom33, a novel transmembrane nucleoporin required for proper nuclear pore complex distribution. *J. Cell Biol.* 189:795–811. http://dx.doi.org/10.1083/jcb.200910043

Chung, S., and P.A. Takizawa. 2010. Multiple Myo4 motors enhance ASH1 mRNA transport in *Saccharomyces cerevisiae*. *J. Cell Biol.* 189:755–767. http://dx.doi.org/10.1083/jcb.200912011

Cox, J., and M. Mann. 2008. MaxQuant enables high peptide identification rates, individualized p.p.b.-range mass accuracies and proteome-wide protein quantification. *Nat. Biotechnol.* 26:1367–1372. http://dx.doi.org/10.1038/nbt.1511

Cox, J., N. Neuhauser, A. Michalski, R.A. Scheltema, J.V. Olsen, and M. Mann. 2011. Andromeda: a peptide search engine integrated into the MaxQuant environment. *J. Proteome Res.* 10:1794–1805. http://dx.doi.org/10.1021/pr101065j

Cronshaw, J.M., A.N. Krutchinsky, W. Zhang, B.T. Chait, and M.J. Matunis. 2002. Proteomic analysis of the mammalian nuclear pore complex. *J. Cell Biol.* 158:915–927. http://dx.doi.org/10.1083/jcb.200206106

D'Angelo, M.A., M. Raices, S.H. Panowski, and M.W. Hetzer. 2009. Age-dependent deterioration of nuclear pore complexes causes a loss of nuclear integrity in postmitotic cells. *Cell.* 136:284–295. http://dx.doi.org/10.1016/j.cell.2008.11.037

D'Angelo, M.A., J.S. Gomez-Cavazos, A. Mei, D.H. Lackner, and M.W. Hetzer. 2012. A change in nuclear pore complex composition regulates cell differentiation. *Dev. Cell.* 22:446–458. http://dx.doi.org/10.1016/j.devcel.2011.11.021

Daigle, N., J. Beaudouin, L. Hartnell, G. Imreh, E. Hallberg, J. Lippincott-Schwartz, and J. Ellenberg. 2001. Nuclear pore complexes form immobile networks and have a very low turnover in live mammalian cells. *J. Cell Biol.* 154:71–84. http://dx.doi.org/10.1083/jcb.200101089

Dawson, T.R., M.D. Lazarus, M.W. Hetzer, and S.R. Wente. 2009. ER membrane-bending proteins are necessary for de novo nuclear pore formation. *J. Cell Biol.* 184:659–675. http://dx.doi.org/10.1083/jcb.200806174

de Jong-Curtain, T.A., A.C. Parslow, A.J. Trotter, N.E. Hall, H. Verkade, T. Tabone, E.L. Christie, M.O. Crowhurst, J.E. Layton, I.T. Shepherd, et al. 2009. Abnormal nuclear pore formation triggers apoptosis in the intestinal epithelium of elys-deficient zebrafish. *Gastroenterology.* 136:902–911. http://dx.doi.org/10.1053/j.gastro.2008.11.012

Doucet, C.M., J.A. Talamas, and M.W. Hetzer. 2010. Cell cycle-dependent differences in nuclear pore complex assembly in metazoa. *Cell.* 141:1030–1041. http://dx.doi.org/10.1016/j.cell.2010.04.036

Du, Y., M. Pypaert, P. Novick, and S. Ferro-Novick. 2001. Aux1p/Swa2p is required for cortical endoplasmic reticulum inheritance in *Saccharomyces cerevisiae*. *Mol. Biol. Cell.* 12:2614–2628. http://dx.doi.org/10.1091/mbc.12.9.2614

Dultz, E., and J. Ellenberg. 2010. Live imaging of single nuclear pores reveals unique assembly kinetics and mechanism in interphase. *J. Cell Biol.* 191:15–22. http://dx.doi.org/10.1083/jcb.201007076

Eshel, D., L.A. Urrestarazu, S. Vissers, J.C. Jauniaux, J.C. van Vliet-Reedijk, R.J. Planta, and I.R. Gibbons. 1993. Cytoplasmic dynein is required for normal nuclear segregation in yeast. *Proc. Natl. Acad. Sci. USA.* 90:11172–11176. http://dx.doi.org/10.1073/pnas.90.23.11172

Estrada, P., J. Kim, J. Coleman, L. Walker, B. Dunn, P. Takizawa, P. Novick, and S. Ferro-Novick. 2003. Myo4p and She3p are required for cortical ER inheritance in *Saccharomyces cerevisiae*. *J. Cell Biol.* 163:1255–1266. http://dx.doi.org/10.1083/jcb.200304030

Eves, P.T., Y. Jin, M. Brunner, and L.S. Weisman. 2012. Overlap of cargo binding sites on myosin V coordinates the inheritance of diverse cargoes. *J. Cell Biol.* 198:69–85. http://dx.doi.org/10.1083/jcb.201201024

Fagarasanu, A., M. Fagarasanu, G.A. Eitzen, J.D. Aitchison, and R.A. Rachubinski. 2006. The peroxisomal membrane protein Inp2p is the peroxisome-specific receptor for the myosin V motor Myo2p of *Saccharomyces cerevisiae*. *Dev. Cell.* 10:587–600. http://dx.doi.org/10.1016/j.devcel.2006.04.012

Fehrenbacher, K.L., D. Davis, M. Wu, I. Boldogh, and L.A. Pon. 2002. Endoplasmic reticulum dynamics, inheritance, and cytoskeletal interactions in budding yeast. *Mol. Biol. Cell.* 13:854–865. http://dx.doi.org/10.1091/mbc.01-04-0184

Fichtman, B., C. Ramos, B. Rasala, A. Harel, and D.J. Forbes. 2010. Inner/outer nuclear membrane fusion in nuclear pore assembly: biochemical demonstration and molecular analysis. *Mol. Biol. Cell.* 21:4197–4211. http://dx.doi.org/10.1091/mbc.E10-04-0309

Fröhlich, F., R. Christiano, and T.C. Walther. 2013. Native SILAC: metabolic labeling of proteins in prototroph microorganisms based on lysine synthesis regulation. *Mol. Cell. Proteomics.* 12:1995–2005. http://dx.doi.org/10.1074/mcp.M112.025742

Gomez-Ospina, N., G. Morgan, T.H. Giddings Jr., B. Kosova, E. Hurt, and M. Winey. 2000. Yeast nuclear pore complex assembly defects determined by nuclear envelope reconstruction. *J. Struct. Biol.* 132:1–5. http://dx.doi.org/10.1006/jsbi.2000.4305

Goode, B.L., A.A. Rodal, G. Barnes, and D.G. Drubin. 2001. Activation of the Arp2/3 complex by the actin filament binding protein Abp1p. *J. Cell Biol.* 153:627–634. http://dx.doi.org/10.1083/jcb.153.3.627

Grandi, P., V. Doye, and E.C. Hurt. 1993. Purification of NSP1 reveals complex formation with 'GLFG' nucleoporins and a novel nuclear pore protein NIC96. *EMBO J.* 12:3061–3071.

Grandi, P., S. Emig, C. Weise, F. Hucho, T. Pohl, and E.C. Hurt. 1995. A novel nuclear pore protein Nup82p which specifically binds to a fraction of Nsp1p. *J. Cell Biol.* 130:1263–1273. http://dx.doi.org/10.1083/jcb.130.6.1263

Grandi, P., T. Dang, N. Pané, A. Shevchenko, M. Mann, D. Forbes, and E. Hurt. 1997. Nup93, a vertebrate homologue of yeast Nic96p, forms a complex with a novel 205-kDa protein and is required for correct nuclear pore assembly. *Mol. Biol. Cell.* 8:2017–2038. http://dx.doi.org/10.1091/mbc.8.10.2017

Grava, S., F. Schaerer, M. Faty, P. Philippsen, and Y. Barral. 2006. Asymmetric recruitment of dynein to spindle poles and microtubules promotes proper spindle orientation in yeast. *Dev. Cell.* 10:425–439. http://dx.doi.org/10.1016/j.devcel.2006.02.018

Haruki, H., J. Nishikawa, and U.K. Laemmli. 2008. The anchor-away technique: rapid, conditional establishment of yeast mutant phenotypes. *Mol. Cell.* 31:925–932. http://dx.doi.org/10.1016/j.molcel.2008.07.020

Hayakawa, A., A. Babour, L. Sengmanivong, and C. Dargemont. 2012. Ubiquitylation of the nuclear pore complex controls nuclear migration during mitosis in *S. cerevisiae*. *J. Cell Biol.* 196:19–27. http://dx.doi.org/10.1083/jcb.201108124

Hill, K.L., N.L. Catlett, and L.S. Weisman. 1996. Actin and myosin function in directed vacuole movement during cell division in *Saccharomyces cerevisiae*. *J. Cell Biol.* 135:1535–1549. http://dx.doi.org/10.1083/jcb.135.6.1535

Hoepfner, D., M. van den Berg, P. Philippsen, H.F. Tabak, and E.H. Hettema. 2001. A role for Vps1p, actin, and the Myo2p motor in peroxisome abundance and inheritance in *Saccharomyces cerevisiae*. *J. Cell Biol.* 155:979–990. http://dx.doi.org/10.1083/jcb.200107028

Hubert, T., J. Vandekerckhove, and J. Gettemans. 2009. Exo70-mediated recruitment of nucleoporin Nup62 at the leading edge of migrating cells is required for cell migration. *Traffic.* 10:1257–1271. http://dx.doi.org/10.1111/j.1600-0854.2009.00940.x

Iizuka, R., M. Yamagishi-Shirasaki, and T. Funatsu. 2011. Kinetic study of de novo chromophore maturation of fluorescent proteins. *Anal. Biochem.* 414:173–178. http://dx.doi.org/10.1016/j.ab.2011.03.036

Itoh, T., A. Watabe, A. Toh-E, and Y. Matsui. 2002. Complex formation with Ypt11p, a rab-type small GTPase, is essential to facilitate the function of Myo2p, a class V myosin, in mitochondrial distribution in *Saccharomyces cerevisiae*. *Mol. Cell. Biol.* 22:7744–7757. http://dx.doi.org/10.1128/MCB.22.22.7744-7757.2002

Kessel, R.G. 1992. Annulate lamellae: a last frontier in cellular organelles. *Int. Rev. Cytol.* 133:43–120. http://dx.doi.org/10.1016/S0074-7696(08)61858-6

Khmelinskii, A., P.J. Keller, H. Lorenz, E. Schiebel, and M. Knop. 2010. Segregation of yeast nuclear pores. *Nature*. 466:E1. http://dx.doi.org/10.1038/nature09255

Khmelinskii, A., P.J. Keller, A. Bartosik, M. Meurer, J.D. Barry, B.R. Mardin, A. Kaufmann, S. Trautmann, M. Wachsmuth, G. Pereira, et al. 2012. Tandem fluorescent protein timers for in vivo analysis of protein dynamics. *Nat. Biotechnol.* 30:708–714. http://dx.doi.org/10.1038/nbt.2281

Kirchenbauer, M., and D. Liakopoulos. 2013. An auxiliary, membrane-based mechanism for nuclear migration in budding yeast. *Mol. Biol. Cell.* 24:1434–1443. http://dx.doi.org/10.1091/mbc.E12-08-0602

Korinek, W.S., M.J. Copeland, A. Chaudhuri, and J. Chant. 2000. Molecular linkage underlying microtubule orientation toward cortical sites in yeast. *Science*. 287:2257–2259. http://dx.doi.org/10.1126/science.287.5461.2257

Kosova, B., N. Panté, C. Rollenhagen, and E. Hurt. 1999. Nup192p is a conserved nucleoporin with a preferential location at the inner site of the nuclear membrane. *J. Biol. Chem.* 274:22646–22651. http://dx.doi.org/10.1074/jbc.274.32.22646

Li, Y.Y., E. Yeh, T. Hays, and K. Bloom. 1993. Disruption of mitotic spindle orientation in a yeast dynein mutant. *Proc. Natl. Acad. Sci. USA*. 90:10096–10100. http://dx.doi.org/10.1073/pnas.90.21.10096

Liang, C., M. Weinreich, and B. Stillman. 1995. ORC and Cdc6p interact and determine the frequency of initiation of DNA replication in the genome. *Cell*. 81:667–676. http://dx.doi.org/10.1016/0092-8674(95)90528-6

Logie, C., and A.F. Stewart. 1995. Ligand-regulated site-specific recombination. *Proc. Natl. Acad. Sci. USA*. 92:5940–5944. http://dx.doi.org/10.1073/pnas.92.13.5940

Lupu, F., A. Alves, K. Anderson, V. Doye, and E. Lacy. 2008. Nuclear pore composition regulates neural stem/progenitor cell differentiation in the mouse embryo. *Dev. Cell*. 14:831–842. http://dx.doi.org/10.1016/j.devcel.2008.03.011

Maeshima, K., H. Iino, S. Hihara, T. Funakoshi, A. Watanabe, M. Nishimura, R. Nakatomi, K. Yahata, F. Imamoto, T. Hashikawa, et al. 2010. Nuclear pore formation but not nuclear growth is governed by cyclin-dependent kinases (Cdks) during interphase. *Nat. Struct. Mol. Biol.* 17:1065–1071. http://dx.doi.org/10.1038/nsmb.1878

Makio, T., L.H. Stanton, C.-C. Lin, D.S. Goldfarb, K. Weis, and R.W. Wozniak. 2009. The nucleoporins Nup170p and Nup157p are essential for nuclear pore complex assembly. *J. Cell Biol.* 185:459–473. http://dx.doi.org/10.1083/jcb.200810029

Marelli, M., J.D. Aitchison, and R.W. Wozniak. 1998. Specific binding of the karyopherin Kap121p to a subunit of the nuclear pore complex containing Nup53p, Nup59p, and Nup170p. *J. Cell Biol.* 143:1813–1830. http://dx.doi.org/10.1083/jcb.143.7.1813

Maul, G.G., H.M. Maul, J.E. Scogna, M.W. Lieberman, G.S. Stein, B.Y. Hsu, and T.W. Borun. 1972. Time sequence of nuclear pore formation in phytohemagglutinin-stimulated lymphocytes and in HeLa cells during the cell cycle. *J. Cell Biol.* 55:433–447. http://dx.doi.org/10.1083/jcb.55.2.433

McMillan, J.N., R.A. Sia, E.S. Bardes, and D.J. Lew. 1999. Phosphorylation-independent inhibition of Cdc28p by the tyrosine kinase Swe1p in the morphogenesis checkpoint. *Mol. Cell. Biol.* 19:5981–5990.

Miller, R.K., S.C. Cheng, and M.D. Rose. 2000. Bim1p/Yeb1p mediates the Kar9p-dependent cortical attachment of cytoplasmic microtubules. *Mol. Biol. Cell*. 11:2949–2959. http://dx.doi.org/10.1091/mbc.11.9.2949

Mutvei, A., S. Dihlmann, W. Herth, and E.C. Hurt. 1992. NSP1 depletion in yeast affects nuclear pore formation and nuclear accumulation. *Eur. J. Cell Biol.* 59:280–295.

Nehrbass, U., H. Kern, A. Mutvei, H. Horstmann, B. Marshallsay, and E.C. Hurt. 1990. NSP1: a yeast nuclear envelope protein localized at the nuclear pores exerts its essential function by its carboxy-terminal domain. *Cell*. 61:979–989. http://dx.doi.org/10.1016/0092-8674(90)90063-K

Neumüller, R.A., and J.A. Knoblich. 2009. Dividing cellular asymmetry: asymmetric cell division and its implications for stem cells and cancer. *Genes Dev*. 23:2675–2699. http://dx.doi.org/10.1101/gad.1850809

Onischenko, E., L.H. Stanton, A.S. Madrid, T. Kieselbach, and K. Weis. 2009. Role of the Ndc1 interaction network in yeast nuclear pore complex assembly and maintenance. *J. Cell Biol.* 185:475–491. http://dx.doi.org/10.1083/jcb.200810030

Prinz, W.A., L. Grzyb, M. Veenhuis, J.A. Kahana, P.A. Silver, and T.A. Rapoport. 2000. Mutants affecting the structure of the cortical endoplasmic reticulum in *Saccharomyces cerevisiae*. *J. Cell Biol.* 150:461–474. http://dx.doi.org/10.1083/jcb.150.3.461

Pruyne, D., A. Legesse-Miller, L. Gao, Y. Dong, and A. Bretscher. 2004. Mechanisms of polarized growth and organelle segregation in yeast. *Annu. Rev. Cell Dev. Biol.* 20:559–591. http://dx.doi.org/10.1146/annurev.cellbio.20.010403.103108

Rappsilber, J., W.J. Friesen, S. Paushkin, G. Dreyfuss, and M. Mann. 2003. Detection of arginine dimethylated peptides by parallel precursor ion scanning mass spectrometry in positive ion mode. *Anal. Chem.* 75:3107–3114. http://dx.doi.org/10.1021/ac026283q

Rossanese, O.W., C.A. Reinke, B.J. Bevis, A.T. Hammond, I.B. Sears, J. O'Connor, and B.S. Glick. 2001. A role for actin, Cdc1p, and Myo2p in the inheritance of late Golgi elements in *Saccharomyces cerevisiae*. *J. Cell Biol.* 153:47–62. http://dx.doi.org/10.1083/jcb.153.1.47

Rout, M.P., J.D. Aitchison, A. Suprapto, K. Hjertaas, Y. Zhao, and B.T. Chait. 2000. The yeast nuclear pore complex: composition, architecture, and transport mechanism. *J. Cell Biol.* 148:635–651. http://dx.doi.org/10.1083/jcb.148.4.635

Savas, J.N., B.H. Toyama, T. Xu, J.R. Yates III, and M.W. Hetzer. 2012. Extremely long-lived nuclear pore proteins in the rat brain. *Science*. 335:942. http://dx.doi.org/10.1126/science.1217421

Schindelin, J., I. Arganda-Carreras, E. Frise, V. Kaynig, M. Longair, T. Pietzsch, S. Preibisch, C. Rueden, S. Saalfeld, B. Schmid, et al. 2012. Fiji: an open-source platform for biological-image analysis. *Nat. Methods*. 9:676–682. http://dx.doi.org/10.1038/nmeth.2019

Schlaich, N.L., M. Häner, A. Lustig, U. Aebi, and E.C. Hurt. 1997. In vitro reconstitution of a heterotrimeric nucleoporin complex consisting of recombinant Nsp1p, Nup49p, and Nup57p. *Mol. Biol. Cell*. 8:33–46. http://dx.doi.org/10.1091/mbc.8.1.33

Shcheprova, Z., S. Baldi, S.B. Frei, G. Gonnet, and Y. Barral. 2008. A mechanism for asymmetric segregation of age during yeast budding. *Nature*. 454:728–734.

Sia, R.A., E.S. Bardes, and D.J. Lew. 1998. Control of Swe1p degradation by the morphogenesis checkpoint. *EMBO J.* 17:6678–6688. http://dx.doi.org/10.1093/emboj/17.22.6678

Sikorski, R.S., and P. Hieter. 1989. A system of shuttle vectors and yeast host strains designed for efficient manipulation of DNA in *Saccharomyces cerevisiae*. *Genetics*. 122:19–27.

Siniossoglou, S., C. Wimmer, M. Rieger, V. Doye, H. Tekotte, C. Weise, S. Emig, A. Segref, and E.C. Hurt. 1996. A novel complex of nucleoporins, which includes Sec13p and a Sec13p homolog, is essential for normal nuclear pores. *Cell*. 84:265–275. http://dx.doi.org/10.1016/S0092-8674(00)80981-2

Siniossoglou, S., M. Lutzmann, H. Santos-Rosa, K. Leonard, S. Mueller, U. Aebi, and E. Hurt. 2000. Structure and assembly of the Nup84p complex. *J. Cell Biol.* 149:41–54. http://dx.doi.org/10.1083/jcb.149.1.41

Splinter, D., M.E. Tanenbaum, A. Lindqvist, D. Jaarsma, A. Flotho, K.L. Yu, I. Grigoriev, D. Engelsma, E.D. Haasdijk, N. Keijzer, et al. 2010. Bicaudal D2, dynein, and kinesin-1 associate with nuclear pore complexes and regulate centrosome and nuclear positioning during mitotic entry. *PLoS Biol.* 8:e1000350. http://dx.doi.org/10.1371/journal.pbio.1000350

Steinberg, G., M. Schuster, U. Theisen, S. Kilaru, A. Forge, and M. Martin-Urdiroz. 2012. Motor-driven motility of fungal nuclear pores organizes chromosomes and fosters nucleocytoplasmic transport. *J. Cell Biol.* 198:343–355. http://dx.doi.org/10.1083/jcb.201201087

Stelter, P., R. Kunze, D. Flemming, D. Höpfner, P. Diepholz, P. Philippsen, B. Böttcher, and E. Hurt. 2007. Molecular basis for the functional interaction of dynein light chain with the nuclear-pore complex. *Nat. Cell Biol.* 9:788–796. http://dx.doi.org/10.1038/ncb1604

Talamas, J.A., and M.W. Hetzer. 2011. POM121 and Sun1 play a role in early steps of interphase NPC assembly. *J. Cell Biol.* 194:27–37. http://dx.doi.org/10.1083/jcb.201012154

Vasu, S., S. Shah, A. Orjalo, M. Park, W.H. Fischer, and D.J. Forbes. 2001. Novel vertebrate nucleoporins Nup133 and Nup160 play a role in mRNA export. *J. Cell Biol.* 155:339–354. http://dx.doi.org/10.1083/jcb.200108007

Verzijlbergen, K.F., V. Menendez-Benito, T. van Welsem, S.J. van Deventer, D.L. Lindstrom, H. Ovaa, J. Neefjes, D.E. Gottschling, and F. van Leeuwen. 2010. Recombination-induced tag exchange to track old and new proteins. *Proc. Natl. Acad. Sci. USA*. 107:64–68. http://dx.doi.org/10.1073/pnas.0911164107

Vollmer, B., A. Schooley, R. Sachdev, N. Eisenhardt, A.M. Schneider, C. Sieverding, J. Madlung, U. Gerken, B. Macek, and W. Antonin. 2012.

Dimerization and direct membrane interaction of Nup53 contribute to nuclear pore complex assembly. *EMBO J.* 31:4072–4084. http://dx.doi .org/10.1038/emboj.2012.256

Wesp, A., L. Hicke, J. Palecek, R. Lombardi, T. Aust, A.L. Munn, and H. Riezman. 1997. End4p/Sla2p interacts with actin-associated proteins for endocytosis in *Saccharomyces cerevisiae*. *Mol. Biol. Cell*. 8:2291–2306. http://dx.doi.org/10.1091/mbc.8.11.2291

Winey, M., D. Yarar, T.H. Giddings Jr., and D.N. Mastronarde. 1997. Nuclear pore complex number and distribution throughout the *Saccharomyces cerevisiae* cell cycle by three-dimensional reconstruction from electron micrographs of nuclear envelopes. *Mol. Biol. Cell*. 8:2119–2132. http:// dx.doi.org/10.1091/mbc.8.11.2119

Yang, H.-C., and L.A. Pon. 2002. Actin cable dynamics in budding yeast. *Proc. Natl. Acad. Sci. USA*. 99:751–756. http://dx.doi.org/10.1073/ pnas.022462899

Yang, H.C., A. Palazzo, T.C. Swayne, and L.A. Pon. 1999. A retention mechanism for distribution of mitochondria during cell division in budding yeast. *Curr. Biol.* 9:1111–1114. http://dx.doi.org/10.1016/ S0960-9822(99)80480-1

Yewdell, W.T., P. Colombi, T. Makhnevych, and C.P. Lusk. 2011. Lumenal interactions in nuclear pore complex assembly and stability. *Mol. Biol. Cell*. 22:1375–1388. http://dx.doi.org/10.1091/mbc.E10-06-0554

Yin, H., D. Pruyne, T.C. Huffaker, and A. Bretscher. 2000. Myosin V orientates the mitotic spindle in yeast. *Nature*. 406:1013–1015. http://dx.doi .org/10.1038/35023024

Zabel, U., V. Doye, H. Tekotte, R. Wepf, P. Grandi, and E.C. Hurt. 1996. Nic96p is required for nuclear pore formation and functionally interacts with a novel nucleoporin, Nup188p. *J. Cell Biol.* 133:1141–1152. http://dx.doi .org/10.1083/jcb.133.6.1141

Zhang, L., N.G. Gurskaya, E.M. Merzlyak, D.B. Staroverov, N.N. Mudrik, O.N. Samarkina, L.M. Vinokurov, S. Lukyanov, and K.A. Lukyanov. 2007. Method for real-time monitoring of protein degradation at the single cell level. *Biotechniques*. 42:446–450. http://dx.doi.org/10.2144/000112453